Stability of Pipes Subjected to Fluid Flow Induced Vibration with Flexible Boundary Conditions in Discharge

by

Giorgio Costa Del Pozo

Under the supervision of

Professor Michael P. Paidoussis

Department of Mechanical Engineering

McGill University

Montréal, Québec, Canada

A thesis submitted to McGill University in partial fulfillment
of the requirements of the Undergraduate Honours Program

Abstract

The dynamics of pipes conveying fluid are of great interest not only fundamentally for the field of fluid-structure interactions but also to the resource extraction and excavation industries. However, rarely may systems be described by ideal boundary conditions such as perfectly clamped or pinned. The focus of this thesis is to develop a model with flexible boundary conditions and to use it to better understand the dynamics of pipes conveying fluid with these types of boundary conditions.

The study begins by stating and briefly explaining the methods used to attain a solution and later deriving the mechanics that dictate the motion of a pipe conveying fluid. This produces an equation which is subsequently solved for different sets of boundary conditions, yielding a complete mathematical model of the dynamics of a pipe. Selected standard cases are then deeply analysed to develop two different flexible models. These models are produced by using springs to constrain the motion of a pipe at the origin. Their behaviour with relation to the stiffness of these springs is then studied and explained by comparison to literature. Lastly, an experiment is then qualitatively conducted to have a better understanding of the subject being studied.

As the results illustrate, the models produced are shown to work, with one of them being fully developed while the other having certain limitations. The results suggest that stiffness may have a negative impact on overall stability of a pipe conveying fluid.

Sommaire

La dynamique des tuyaux déchargeant du fluide est d'un grand intérêt non seulement dans le domaine des interactions fluide-structure, mais aussi pour l'extraction des ressources naturelles. Rarement les systèmes sont décrits par de conditions-limites idéales, comme, par exemple, parfaitement supports encastrés ou supports simples. L'objectif de cette thèse était de développer un modèle avec des conditions-limites flexibles et utiliser ces modèles pour comprendre la dynamique des tuyaux quand ils déchargeant du fluide avec ces types de conditions aux limites.

Le projet a commencé par une explication brève des méthodes utilisées pour arriver à une solution et ensuite la dérivation d'un modèle pour le mouvement d'un tuyau parcoure par un fluide. L'équation produit a été résolu pour de différents ensembles de conditions-limites, ce qui donne un modèle mathématique complet de la dynamique du tuyau. Configurations classiques des conditions-limites ont été analysées en profondeur pour développer deux modèles flexibles différents. Elles ont été créées en utilisant des ressorts qui limitent le mouvement du tuyau à l'origine. Le comportement par rapport à la rigidité de ces ressorts a été étudié et expliqué en comparaison avec la littérature existante. Une expérience a été effectuée qualitativement pour une meilleure compréhension du domaine d'étude.

Le projet a montré que les modèles fonctionnent bien; l'un étant entièrement développé tandis que l'autre ayant certaines limitations. Il a été montré que la rigidité accrue peut être déstabilisante pour le tuyau parcoure par un fluide.

Acknowledgements

First of all, I would like to give my most profound thanks to my thesis supervisor, Professor Michael P. Paidoussis, for all of his help and guidance throughout the entire duration of the thesis. His constant encouragement and interest in my work was a constant motivation to do my best.

Next, I would like to thank my dear friend Kyriakos for always being supportive while we worked at the laboratory on our corresponding theses. Without his companionship I would have probably gone mad inside the lab.

I would also like to extend my thanks to all the members of the fluid-structure interactions lab at McGill University, especially Mojtaba and Mergen for their help and support with the project.

I cannot be thankful enough to my loving girlfriend Lauren Hudak whose support throughout this entire year was heartening, as well as for helping me review my thesis, which I would have not entrusted with anybody else.

A special mention goes to my friend Thomas Friedlaender, who sacrificed his own time to produce the LabVIEW ® program used during the thesis.

Finally, but most importantly, I would like to thank my parents – Luis and Marion – and my sister – Antonella – for all of their love and support through all the years that I have been away. I miss them dearly but I always carry them in my heart. Their constant effort to support me while I endeavoured in my studies was an inspiration. I would like to dedicate this thesis to them.

Table of Contents

Chapter 1
Introduction

1.1 Purpose of the Research

The intent of this research is to study the dynamics and stability of slender, vertical pipes conveying fluid with flexible boundary conditions during discharge. These peculiar boundary conditions are intended to model more realistic situations where slender pipes are involved, such as offshore drilling. The objective is to identify and predict the fluid flow velocities which lead to self-excited oscillations, using a theoretical approach based on a mathematical model. The models will then be compared qualitatively to experimental results.

For the purpose of this thesis two different cases with flexible boundary conditions will be considered. The first will be a pinned-free pipe with a rotational spring placed at the origin. This spring will add stiffness and constrain motion, so that the model behaves as one intermediate between the two standard cases of pinned-free and clamped-free (cantilever) boundary conditions. Taking the previous concept a step further, the second case to be developed consists of a free-free pipe with both a rotational and a translational spring at the origin. Based on the stiffness given to each spring, this set-up should provide the possibility of producing hybrid boundary conditions between the standard cases of clamped-free, pinned-free and free-free. Ideally, two working mathematical models will be developed to reproduce and analyse the dynamic behaviour of the aforementioned cases with flexible boundary conditions. The models will be compared with models of the standard cases to judge their reliability.

Further, an experiment will then be conducted to test the models produced in this investigation. However, due to time constraints and the complexity of flexible boundary conditions, the experiment will only test a clamped-free configuration. The experiment will only produce qualitative results to better understand the overall behaviour of loss of stability.

The final objective will be to use the information obtained, both by mathematical models and by experimentation, to generate and verify the critical fluid-flow velocities at which instabilities occur for these flexible boundary conditions. This is important not only theoretically but also in application since these are more 'realistic' conditions. There has been ample research done on fluid-flow induced vibration, but boundary conditions are always assumed to be ideal, such as perfectly clamped.

However, this is not always an appropriate approximation. In other words, many applications boundaries tend to be flexible. This project will attempt to create a model with variable spring stiffness, and then observe, validate, and understand how such a system with these flexible (non-ideal) boundary conditions behaves during discharge.

1.2 Outline of the Thesis

The main objective of the thesis is to identify the fluid flow velocities leading to instabilities in pipes with flexible boundary conditions (with a 'flexible'-free configuration). The approach is mostly theoretical due to the complexity of designing an experimental set-up to appropriately test flexible conditions.

The thesis is divided into four chapters. The first chapter describes the motivation and intent of the research by providing some examples of industrial applications and describing the basics of the problem. This is followed by a detailed description of the methods used by the author to

solve the problem and develop the theoretical model. Chapter 2 considers, rather selectively than extensively, examples of cases of dynamics of pipes conveying fluid. The examples are used as benchmarks for the flexible models developed. Chapter 3 starts by explaining the development of the models with flexible boundary conditions, and then presenting the influence of flexibility on the stability of the pipes (using critical flow velocity as an indicator). Chapter 4 describes the experiment performed to compare against the theoretical predictions. Finally, chapter 5 concludes with an overview of the findings in addition to recommendations for future research.

1.3 Industrial Interest

The motivation for this thesis is not only academic but also practical. The field of fluid-structure interactions can be observed not only in many engineering systems, but also in nature. The problems that arise can be very complex. Therefore, being able to better simulate natural conditions may also generate a better understanding of the subject. When considering that the applications from this research range from ocean mining to the towing of flexible barges, the application of flexible boundary conditions allows for a better approach when modelling an existing system to better understand its dynamics. Even though self-excited vibrations may sometimes be desirable in some cases, such as in ichthyoid propulsion systems, it can also be very detrimental to equipment and infrastructure, and even to human life.

1.4 Methods of Solution

A system in which fluids and structures interact is not easily described. The nonlinear nature of the system would render computing a direct analytical solution of the continuous system overwhelmingly difficult to derive and compute. To overcome this complexity, the system of a pipe conveying fluid flow will be modeled as a linear system, behaving as an Euler-Bernoulli beam with internal flow. As such, three steps (methods) will be used in combination to achieve a

solution of the system. These are (i) the method of separation of variables, (ii) the Galerkin method, (iii) the matrix formulation method for linear systems, and (iv) the presentation of the results.

The first method is applied to produce a set of functions that describe the modes of vibration corresponding to a set of given boundary conditions. The results may then be introduced into the Galerkin method, which converts the problem from continuous to discrete. Finally, the discrete system may be converted to a system of matrices to which linear manipulation can be applied to arrive at a solution yielding the dynamics of the problem.

1.4.1 Separation of Variables for an Euler-Bernoulli Beam

Starting with the Euler-Bernoulli equation of motion for a beam

$$EI\frac{\partial^4 w}{\partial x^4} + m\frac{\partial^2 w}{\partial t^2} = 0\,, \tag{1.1}$$

where $w(x,t)$ is the lateral deflection of the beam, E is the Young's modulus, I is the second moment of area, and m is the mass per unit length for a beam (or pipe) of length L. The terms E and I are assumed to be constant. The problem is completed by a set of four boundary conditions. These are either geometrical or natural boundary conditions. Geometrical boundary conditions account for both displacement and angle, while natural boundary conditions deal with shear forces and moments. The beam describes the free response of a beam undergoing vibration. In order to find a solution to the Euler-Bernoulli equation, separation of variables is applied in the following fashion

$$
\begin{aligned}
w(x,t) &= X(x)\,T(t),\\
\Omega^2 &= \frac{EI}{mL^4}(\lambda L)^4\,,\\
T(t) &= Ae^{i\Omega t},\\
X(x) &= B_1\cos(\lambda x) + B_2\sin(\lambda x) + B_3\cosh(\lambda x) + B_4\sinh(\lambda x)\,,
\end{aligned}
\tag{1.2}
$$

where λ corresponds to the eigenvalues of the mode shape and Ω to the frequency of vibration. Equation (1.2) yields a general solution for both the temporal and spatial components of $w(x,t)$. As an example, consider the boundary conditions of a cantilevered beam (clamped-free) in terms of $w(x,t)$ and then rewritten in terms of the spatial component $X(x)$,

$$
\begin{aligned}
&w|_{x=0} = 0\,,\ \ \frac{\partial w}{\partial x}|_{x=0} = 0\,,\ \ EI\frac{\partial^2 w}{\partial x^2}|_{x=L} = 0\,,\ \ EI\frac{\partial^3 w}{\partial x^3}|_{x=L} = 0\,;\\
&X|_{x=0} = 0\,,\ \ \frac{dX}{dx}|_{x=0} = 0\,,\ \ \frac{d^2X}{dx^2}|_{x=L} = 0\,,\ \ \frac{d^3X}{dx^3}|_{x=L} = 0\,.
\end{aligned}
\tag{1.3}
$$

The boundary conditions allow for a solution of the spatial equation by producing four homogeneous equations from which the mode shape and eigenvalues may be obtained. Eliminating three equations, the solution may be expressed in terms of only one constant, here B_3. However, only the mode shape is meaningful. Thus the equation may be normalized by letting $\phi_r(x)$ be the normalized spatial equation. This type of function, from here on, will be referred to as a comparison function and it describes the mode shape of the beam. Hence

$$
\phi_r(x) = \cosh(\lambda_r x) - \cos(\lambda_r x) - \sigma_r[\sinh(\lambda_r x) - \sin(\lambda_r x)]\,, \tag{1.4}
$$

where

$$
\sigma_r = \frac{\sinh(\lambda_r L) - \sin(\lambda_r L)}{\cosh(\lambda_r L) + \cos(\lambda_r L)}, \tag{1.5}
$$

and the corresponding modal frequencies, or eigenvalues, are found through the characteristic equation

$$\cos(\lambda_r L)\cosh(\lambda_r L) + 1 = 0\,. \tag{1.6}$$

Once the comparison functions and the characteristic equation are defined, it is possible to then discretize the system.

1.4.2 Discretization of the Problem via the Galerkin Method

The Galerkin method, named after the Russian mathematician Boris Galerkin, works by converting continuous systems into discrete ones. It can be related to finite element techniques. A simple example is provided in order to explain the derivation and set-up of the algorithm. Consider a beam, supported as in Figure 1.1

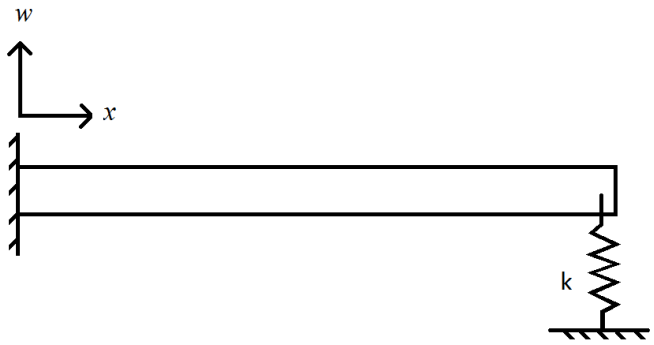

Figure 1.1 - Cantilevered beam with spring at x = L

The figure shows a modified cantilevered beam, with a translational spring (with spring constant *k*) at the normally free end. Thus, the system can be described by the equation of motion (EOM)

$$F(w) = EI\frac{\partial^4 w}{\partial x^4} + m\frac{\partial^2 w}{\partial t^2} + kw\delta_D(x - L) = 0\,, \tag{1.7}$$

where $\delta_D(x - L)$ is the Dirac delta function, which describes the effect of the spring at a given point. Since the spring is accounted for in the EOM, the boundary conditions are those of a standard cantilevered beam, as shown in equation (1.3). A solution of the following form is assumed

$$w(x,t) \cong w_N(x,t) = \sum_{r=1}^{N} \phi_r(x) q_r(t) \,, \tag{1.8}$$

where ϕ_r are the comparison functions, q_r are the generalized coordinates of the system being described, and N is the number of modes used in the approximation. The accuracy of the approximate solution, w_N, is dependent on the number of modes used and will increase as N increases. However, this is not an exact solution and its substitution into equation (1.7) will generally yield a small error. It is necessary to impose the following requirement: over the length of the beam, [0, L], this error will vanish. The Galerkin method states that the best way to impose this is

$$\int_0^L \{F(w)\phi_s(x)\}\, dx = 0 \;, \quad \text{for } s = 1, 2, \ldots, N \,. \tag{1.9}$$

This ensures that the resulting approximate solution is accurate based on the number of modes used. From the derivation in equation (1.2) it is also important to recall that

$$\frac{\partial^4 \phi_r}{\partial x} = \lambda_r^4 \phi_r \,. \tag{1.10}$$

Thus, substituting equations (1.8) and (1.9) into (1.7) yields

$$\sum_{r=1}^{N} EI\lambda_r^4 \phi_r q_r + \sum_{r=1}^{N} m\phi_r \frac{\partial^2 q_r}{\partial t^2} + \sum_{r=1}^{N} k\phi_r q_r \partial_D(x-L) = 0 \,. \tag{1.11}$$

The final step is to impose the condition from equation (1.8) to equation (1.10). This produces the following

$$\sum_{r=1}^{N} EI\lambda_r^4 q_r \int_0^L \phi_r \phi_s \, dx + \sum_{r=1}^{N} m \frac{\partial^2 q_r}{\partial t^2} \int_0^L \phi_r \phi_s \, dx + \sum_{r=1}^{N} k q_r \int_0^L \phi_r \phi_s \partial_D(x-L) \, dx = 0 \,. \tag{1.12}$$

At this point it is important to refer to the orthogonal nature of the comparison functions based on their derivation, which leads to the following conclusion

$$\int_0^L \varphi_r \varphi_s \, d\xi = \begin{cases} 0, r \neq s \\ L, r = s \end{cases}. \tag{1.13}$$

From equations (1.11) and (1.12) it is possible to produce a system of N linear equations, for $s = 1, 2, \dots, N$. These can then be converted into a matrix system of the form

$$[M]\{\ddot{q}\} + [K]\{q\} = 0\,. \tag{1.14}$$

The example presented previously describes a conservative system, which is composed only of a mass (or inertial) matrix $[M]$ and a stiffness matrix $[K]$. More complex systems discussed in this thesis will be non-conservative, which include dissipation terms (described by a dissipation matrix, $[C]$). Once the system is described by matrices it may be solved using general linear algebra, described in the following section.

1.4.3 General Solution of a Discrete System

For a general non-conservative system, the Galerkin method would yield the following

$$[M]\{\ddot{q}\} + [C]\{\dot{q}\} + [K]\{q\} = 0\,, \tag{1.15}$$

where $[M]$ represents the mass matrix, $[C]$ the dissipation matrix, and $[K]$ the stiffness matrix. The system can have 'n' degrees of freedom. The system presented is of second order and will be reduced to a first order system by defining a new set of coordinates and square matrices and rewriting the system

$$\{z\} = \begin{Bmatrix} \{\dot{q}\} \\ \{q\} \end{Bmatrix}, \quad [B] = \begin{bmatrix} [0] & [M] \\ [M] & [C] \end{bmatrix}, \quad [E] = \begin{bmatrix} -[M] & [0] \\ [0] & [K] \end{bmatrix}, \tag{1.16}$$
$$[B]\{\dot{z}\} + [E]\{z\} = 0\,.$$

The system can now be pre-multiplied by $[B]^{-1}$ to finally decouple it. This yields the following

$$[Y] = -[B]^{-1}[E]\,,$$
$$\{\dot{z}\} - [Y]\{z\} = \{0\}\,, \tag{1.17}$$

where $[Y]$ is the inverse dynamical matrix of the first order system. Solving the eigenvalue problem for $[Y]$ yields '2n' eigenvalues, occurring in complex conjugate pairs.

$$(\lambda[I] - [Y]) = 0\,. \tag{1.18}$$

Each pair corresponds to one eigenfrequency (Ω) of the second order system [described in equation (1.15)]. However, it must be noted that the values extracted from the system are related by $\lambda_j = i\Omega_j$.

1.4.4 Analysis of Results

The imaginary part of the eigenfrequency corresponds to damping, while the real part corresponds to the frequency of oscillation. The former is of great interest as the system, being non-conservative, may become self-excited and exhibit instabilities if the imaginary part becomes negative. This corresponds to the finding from the derivation shown in equation (1.2), where the time component of the solution $w(x,t) = X(x)T(t)$ has the following form

$$T(t) = Ae^{i\Omega t}\,. \tag{1.19}$$

Thus, if the imaginary component of the frequency is negative the system increases exponentially with respect to time. This is what is referred to as self-excitement, as the closed system gains energy from its surroundings.

Two types of self-excited instabilities are possible for a linear model of a pipe. The system may either lose stability by static divergence $[Re(\Omega) = 0, Im(\Omega) < 0]$, commonly referred to as buckling, or by flutter $[Re(\Omega) \neq 0, Im(\Omega) < 0]$, where the system becomes unstable and oscillatory. Since the pipes of interest for the research are unconstrained at one end,

the system is non-conservative (Paidoussis M. P., 1998). This means the pipes are expected to show a dynamic divergence (flutter).

To some extent, the dynamic behaviour of a system can be observed and described by the nature of its eigenfrequencies (Ω's). An Argand diagram, which plots the real component of a complex variable versus its imaginary component, may therefore be useful at observing the evolution of the dynamics as the fluid flow velocity is increased. The eigenfrequencies of the system are found for a fixed flow velocity. The flow may then be increased and the process repeated to find the next point for the corresponding mode. This then shows the evolution of the modes of vibration as the velocity is increased.

If fluid flow velocity is increased to the point where the imaginary component of frequency of one of the modes becomes negative the system becomes unstable. That particular velocity is referred to as the critical flow velocity, u_{cr}, of the system. Further increasing the flow velocity results in the linear model collapsing and any behaviour described after this point cannot be accurately predicted any more. Thus, the model is only valid up to the first point of instability in the system.

Chapter 2
Dynamics of a Pipe Conveying Fluid

2.1 Derivation of the Equation of Motion

The dynamics of a pipe conveying fluid are described by its equation of motion (EOM). This equation accounts for all inertial and non-inertial terms, the derivation of which is important to note. Both mathematical and physical derivation and understanding of the terms in the EOM will be explained in this section.

Discrete systems typically use Lagrangian methods for its derivation. However, the problem at hand is continuous and should be treated as such during the derivation of the equation of motion. Newtonian methods and Hamilton's principle will be applied to derive the equation of motion. Both methods will be used alternatively in the derivation of each individual term of the EOM. The development of the equation will start from the basic terms from a pipe without flow, to which the fluid-related terms will be added step by step.

2.1.1 Standard Euler-Bernoulli Beam

A general beam equation, which may also be applied to pipes without flow, presents the terms directly related to the properties of the beam due to its cross-sectional shape, material and mass. To derive the terms variational techniques will be applied to Hamilton's principle,

$$\delta \int_{t_1}^{t_2} (T - V + W) dt = 0 \,, \tag{2.1}$$

where δ is the variational operatoror, T is the kinetic energy of the system, V is the potential energy of the system, and W is the work done by forces not accounted in V. To derive the

equation of the basic Euler-Bernoulli beam, the following are the kinetic and potential energies of such a system

$$T = \frac{1}{2}\int_0^L m\left(\frac{\partial w}{\partial t}\right)^2 dx \quad , \quad V = \frac{1}{2}\int_0^L EI\left(\frac{\partial^2 w}{\partial x^2}\right)^2 dx \, . \tag{2.2}$$

Integrating for an interval of time and applying the variational operator yields

$$\delta \int_{t_1}^{t_2}\int_0^L \frac{1}{2}\left[m\left(\frac{\partial w}{\partial t}\right)^2 - EI\left(\frac{\partial^2 w}{\partial x^2}\right)^2\right] dx\, dt \, . \tag{2.3}$$

This process yields the desired equation of motion and a set of standard boundary conditions, which will be explained in greater detail in the subsequent sections. The resulting equation of motion for this problem is

$$m\frac{\partial^2 w}{\partial t^2} + EI\frac{\partial^4 w}{\partial x^4} = 0 \, , \tag{2.4}$$

where the first term defines the inertial force of the beam, and the second term defines the flexural restoring force given by the beam. The variational technique also gives the following as boundary conditions

$$\begin{aligned} &i)\ w|_{x=0} = 0 && ii)\ w|_{x=L} = 0 \\ &iii)\ \frac{\partial w}{\partial x}|_{x=0} = 0 && iv)\ \frac{\partial w}{\partial x}|_{x=L} = 0 \\ &v)\ \frac{\partial^2 w}{\partial x^2}|_{x=0} = 0 && vi)\ \frac{\partial^2 w}{\partial x^2}|_{x=L} = 0 \\ &vii)\ \frac{\partial^3 w}{\partial x^3}|_{x=0} = 0 && viii)\ \frac{\partial^3 w}{\partial x^3}|_{x=L} = 0 \end{aligned} \tag{2.5}$$

It is important to highlight that there are physical constraints to the boundary conditions that may be selected for a given system. Only four conditions are required to make it a well-defined problem, two at each end of the beam. From equation (2.5), (i) and (ii) mean that there is no

displacement, (iii) and (iv) that the slope must be zero, (v) and (vi) that there is no bending moment produced at the given end, and (vii) and (viii) that there is no shear force applied at the corresponding end.

Since in this subsection the mass of the pipe per unit length, m, has been accounted for, it is of great importance to include an explanation of the concept of added mass. Added mass is the term used to describe the effect of the surrounding medium in the dynamics of an object. For example, an oscillating pipe submerged in water will also have to account for the inertial force of displacing water around it. This effect can be modeled by including an additional term for added mass, where for a cylindrical pipe,

$$m_f = \frac{\pi D^2 \rho_f}{4}, \tag{2.6}$$

where m_f corresponds to the added mass per unit length of the fluid, D to the outer diameter of the pipe, and ρ_f to the density of the surrounding fluid. For simplicity, however, during the subsequent derivations it will be assumed that the parameter m accounts for the summation of both the mass of the pipe and the mass of the fluid per unit length.

2.1.2 Newtonian derivation of fluid flow terms

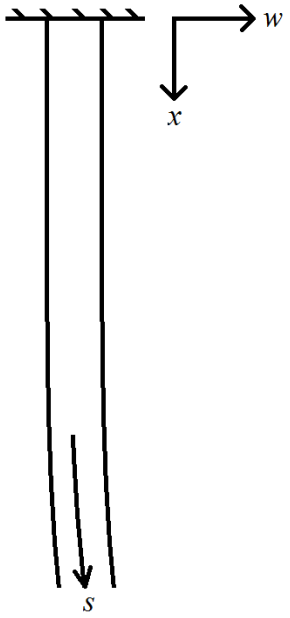

Figure 2.1 – Cantilevered pipe showing the coordinate system, x, y, and s

First of all, it is important to mention that longitudinal (**x**-direction) displacements under consideration are approximately an order of magnitude smaller than lateral ones in the **z**-direction. Thus, during the derivation of the EOM it may be assumed that there is only lateral deflection, as a function of vertical displacement and time, $w = w(x,t)$ (where w represents the motion in the **z**-direction). The fluid flow terms in the equation of motion are derived in from the material derivative. The derivative is applied to the position vector of a fluid flow element. Thus,

$$\boldsymbol{V}_f = \left(\frac{\partial}{\partial t} + U\frac{\partial}{\partial s}\right)(x\boldsymbol{i} + z\boldsymbol{k}) \equiv \frac{D\boldsymbol{r}}{Dt}, \tag{2.7}$$

where U is the fluid flow velocity. The pipe is considered to be inextensible, which is a reasonable assumption since all pipes under consideration have one unconstrained end. This suggests that there is no longitudinal tension, leading to the assumption that $\partial x/\partial t \cong 0$. Moreover, while keeping in mind the assumption of small lateral deflections, it may be said that $\partial x/\partial s \cong 1$. Thus, the expansion of equation (2.7) yields the following

$$\boldsymbol{V}_f = U\boldsymbol{i} + \left[\frac{\partial w}{\partial t} + U\frac{\partial w}{\partial s}\right]\boldsymbol{k}\,. \tag{2.8}$$

Following the same procedure to find the acceleration,

$$\boldsymbol{a}_f = \frac{D^2\boldsymbol{r}}{Dt^2} = \left(\frac{\partial}{\partial t} + U\frac{\partial}{\partial s}\right)\left(U\boldsymbol{i} + \left[\frac{\partial w}{\partial t} + U\frac{\partial w}{\partial s}\right]\boldsymbol{k}\right) = \frac{dU}{dt}\boldsymbol{i} + \left[\frac{\partial}{\partial t} + U\frac{\partial}{\partial s}\right]^2 w\boldsymbol{k}\,. \tag{2.9}$$

Dividing the acceleration of the fluid into its directional components,

$$\boldsymbol{a}_{fk} = \left[\frac{\partial}{\partial t} + U\frac{\partial}{\partial x}\right]^2 w, \quad \boldsymbol{a}_{fi} = \frac{dU}{dt}\,. \tag{2.10}$$

Thus, the fluid-dynamic forces in the lateral direction are

$$F_{fk} = M\left[\frac{\partial}{\partial t} + U\frac{\partial}{\partial x}\right]^2 w = M\frac{\partial^2 w}{\partial t^2} + 2MU\frac{\partial^2 w}{\partial x \partial t} + MU^2\frac{\partial^2 w}{\partial x^2}\,, \tag{2.11}$$

where M is the mass per unit length of the fluid. As previously stated, lateral displacements are an order of magnitude above longitudinal displacements; therefore, these terms describe the dynamic behaviour of the fluid. The first term represents the inertial force produced by the fluid, the second the Coriolis force associated, and the third term the centrifugal force. Combining equations (2.5) and (2.11), the resulting equation of motion is

$$EI\frac{\partial^4 w}{\partial x^4} + 2MU\frac{\partial^2 w}{\partial x \partial t} + MU^2\frac{\partial^2 w}{\partial x^2} + (m+M)\frac{\partial^2 w}{\partial t^2} = 0\,, \tag{2.12}$$

which represents the basic linear EOM of a pipe conveying fluid. However, the complexity of the problem increases once gravity and dissipation (both viscous and viscoelastic) are considered.

2.1.3 The Complete Equation of Motion

The equation shown in (2.12) presents a simplified equation of motion. A better linear model of the dynamics of the pipe conveying fluid may be produced by accounting for dissipation and gravity. Bear in mind that throughout the thesis only pipes with one constrained

end are studied (at the origin). The other end, remains free. This suggests that longitudinal tension in the pipe is non-existent and the pressure difference is negligible.

The viscoelasticity of the pipe may be modeled following dissipation of the Kelvin-Voigt type. This may be represented by replacing the flexural rigidity (EI) of the pipe with the following term

$$\left(E + E^* \frac{\partial}{\partial t}\right) I \frac{\partial^4 w}{\partial x^4}, \tag{2.13}$$

where the above represents a stress-strain relationship of the form $\sigma = E\varepsilon + E^*(d\varepsilon/dt)$. The damping due to friction between the pipe wall and the surrounding fluid then takes the following form

$$c^* \left(\frac{\partial w}{\partial t}\right), \tag{2.14}$$

Where c^* is the damping constant. Finally, the effect of gravity must also be accounted for as the pipe of interest has a vertical configuration. Paidoussis (1998) delineates a careful derivation of the terms by a balance of forces through a Newtonian derivation. Thus, the terms accounting for gravity are

$$(M+m)g\frac{\partial w}{\partial x}\ , \quad (M+m)g(x-L)\frac{\partial^2 w}{\partial x^2}\ . \tag{2.15}$$

Adding all the terms presented above, the following is the complete equation of motion for a pipe in discharge and with one unconstrained end

$$\begin{aligned}\left(E + E^* \frac{\partial}{\partial t}\right) I \frac{\partial^4 w}{\partial x^4} + 2MU\frac{\partial^2 w}{\partial x \partial t} + \{MU^2 + (M+m)g(x-L)\}\frac{\partial^2 w}{\partial x^2} + c^*\frac{\partial w}{\partial t} \\ + (M+m)g\frac{\partial w}{\partial x} + (m+M)\frac{\partial^2 w}{\partial t^2} = 0.\end{aligned} \tag{2.16}$$

The complete EOM presented in equation (2.16) may be nondimensionalized by substituting the following variables into the equation

$$\eta = \frac{w}{L}\,, \quad \xi = \frac{x}{L}\,, \quad \tau = \left(\frac{EI}{m+M}\right)^{\frac{1}{2}} \frac{t}{L^2}\,. \tag{2.17}$$

All other parameters and constants involved are also made dimensionless and the general equation of motion of the system takes the following form

$$\alpha\dot{\eta}'''' + \eta'''' + \{u^2 + \gamma(\xi - 1)\}\eta'' + 2u\beta^{\frac{1}{2}}\dot{\eta}' + \gamma\eta' + \sigma\dot{\eta} + \ddot{\eta} = 0\,, \tag{2.18}$$

where

$$(\,)' = \frac{\partial}{\partial\xi}\,, \quad \dot{(\,)} = \frac{\partial}{\partial\tau}\,, \tag{2.19}$$

and

$$\begin{gathered} u = \left(\frac{M}{EI}\right)^{\frac{1}{2}} UL\,, \quad \beta = \frac{M}{m+M}\,, \quad \gamma = \frac{(M+m)L^3 g}{EI}\,, \\ \alpha = \left[\frac{I}{E(m+M)}\right]^{\frac{1}{2}} \frac{E^*}{L^2}\,, \quad \sigma = \frac{c^* L^2}{[EI(m+M)]^{\frac{1}{2}}}\,. \end{gathered} \tag{2.20}$$

Equation (2.18) will now be the equation of motion used in all the subsequent analysis to produce a solution applicable to more general cases. This equation is generalized to be applicable for pipes with at least one unconstrained end (or 'free' condition) as the effects of tensioning and pressurization are not taken into account, which would be applicable for conservative systems of the type. Note that the nondimensional modal frequency is related to its dimensional counterpart in the following fashion

$$\omega = \left(\frac{M+m}{EI}\right)^{\frac{1}{2}} \Omega L^2\,. \tag{2.21}$$

2.2 Dynamics of Pipes with Classical Boundary Conditions

In this section classic (or standard in literature) boundary conditions will be presented and explained in detail. These will be used as a point of reference for comparison with the models with the flexible boundary conditions developed in Chapter 3. The dynamics of these set-ups will be described by the frequencies of vibrations of the system. They will then be presented in the form of Argand diagrams to not only identify the critical flow velocity but also to observe the evolution of the modes of vibration with increasing fluid flow velocity.

2.2.1 Dynamics of a Pipe with Clamped-Free Boundary Conditions

The first standard case to be discussed is the one of a cantilevered pipe. This particular case has been studied in depth in the past (Gregory & Paidoussis 1966a), and the results obtained will be reproduced and explained for the sake of clarity of this paper. The boundary conditions are

$$X(0) = 0\,,\ \ X'(0) = 0\,,\ \ X''(1) = 0\,,\ \ X'''(1) = 0\,, \tag{2.22}$$

where the clamped boundary condition at the origin shows that there is no displacement and the slope must be zero. The free end yields no shear force or moment. Based on these conditions and using a standard Euler-Bernoulli beam with no flow the comparison functions derived are the following

$$\phi_r(\xi) = \cosh(\lambda_r\xi) - \cos(\lambda_r\xi) - \sigma_r[\sinh(\lambda_r\xi) - \sin(\lambda_r\xi)]\,, \tag{2.23}$$

where

$$\sigma_r = \frac{\sinh(\lambda_r) - \sin(\lambda_r)}{\cosh(\lambda_r) + \cos\,(\lambda_r)}, \tag{2.24}$$

and the characteristic equation is

$$\cos(\lambda_r)\cosh(\lambda_r) + 1 = 0\,. \tag{2.25}$$

The first three mode shapes (ϕ's) were plotted for comparison in Maple ®. Note that in these plots there is no flow through the pipes. They are the normal modes of vibration with no flow.

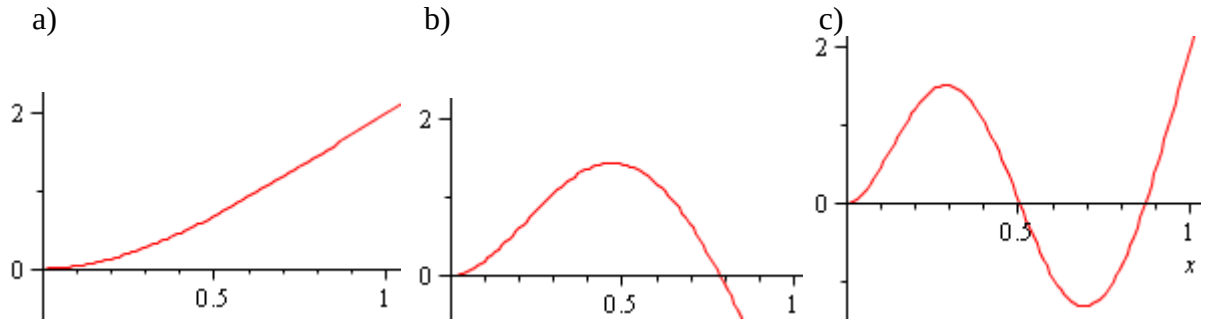

Figure 2.2 – First three modes of vibration for a cantilevered pipe, (a) first mode, (b) second mode, (c) third mode

The Galerkin method is then applied to make the continuous system a discrete one using the equation of motion presented in equation (2.18). The results can then be used to describe the dynamics of the cantilevered pipe.

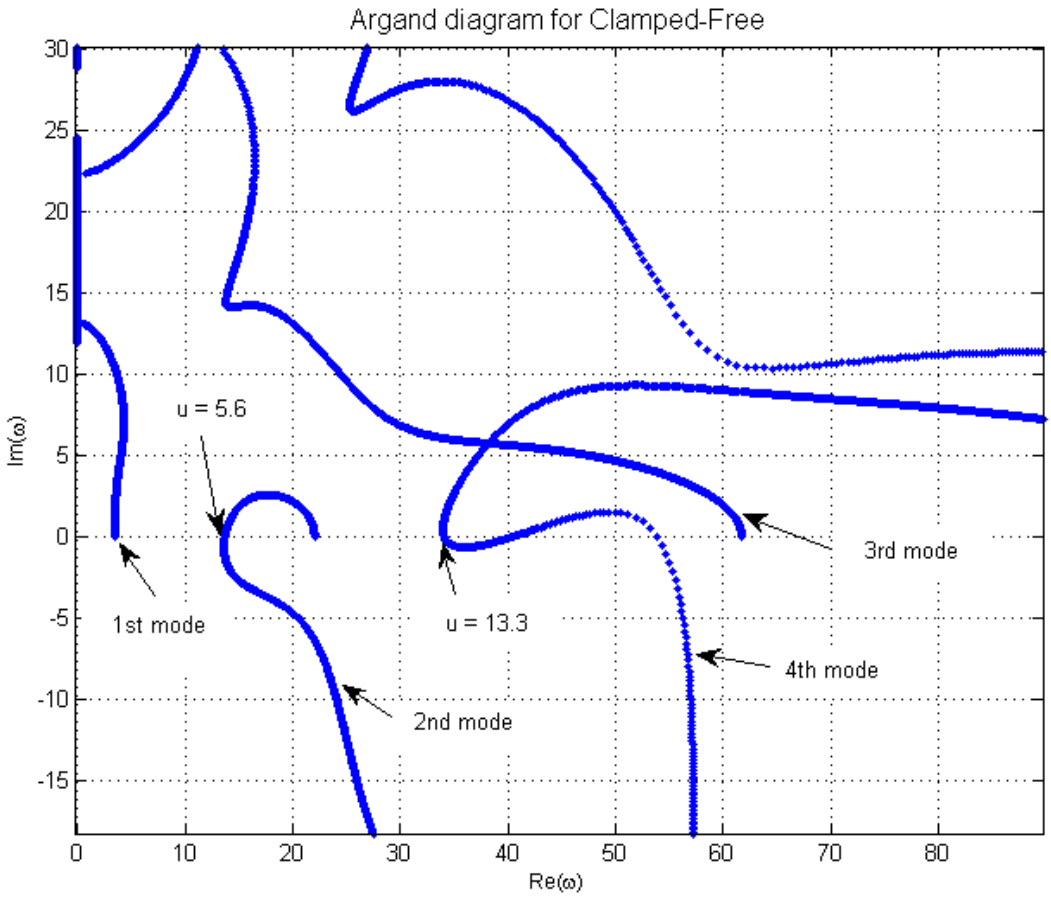

Figure 2.3 – Argand Diagram of a Clamped-Free pipe showing the first four modes for comparison ($\gamma = \alpha = \sigma = 0$) and ($\beta = 0.2$) for $u = 0$ to 18

The parameters selected for the mathematical model $(\beta, \gamma, \sigma, \alpha)$ are obtained from Paidoussis (1998, pg. 112) for a fair comparison of the model against published work. Figure 2.3 shows that the system reaches a critical flow velocity at $u_{cr} = 5.6$. If the velocity is further increased the system becomes unstable by flutter, at which point the linear model collapses and further results cannot be accurately predicted. Nevertheless, the fluid flow velocity at which the first instability occurs for a cantilevered pipe can be predicted by this model. The results highlighted by Figure 2.3 will be used as a benchmark to verify the accuracy of the models with flexible boundary conditions to be described in the subsequent sections.

2.2.2 Dynamics of a Pipe with Pinned-Free Boundary Conditions

Unlike cantilevered pipes, literature regarding the dynamical behaviour for pinned-free supports does not present solutions in the form of Argand diagrams. To be able to carry out a fair comparison with the models for flexible boundary conditions, the dynamics of a pinned-free pipe conveying fluid will be studied in this section.

For a Pinned-Free pipe, the following are the boundary conditions

$$X(0) = 0\,,\;\; X''(0) = 0\,,\;\; X''(1) = 0\,,\;\; X'''(1) = 0\,. \tag{2.26}$$

where the boundary conditions at $\xi = 0$ show that there is no displacement or moment produced by the pinned boundary. The free end behaves like the one presented in the previous section. This particular model has to account for a rigid body mode in the dynamics of the system. The derivation of the mathematical model for this case was itself a challenge, due to the nature of the problem. Due to the pinned constraint the pipe is allowed to rotate freely with no bending. Thus, it exhibits a rigid body mode, which is unrelated to the rest of the bending modes present. During the derivation of the comparison functions, which describe the mode shape of every mode of vibration, it was necessary to account for rigid body motion as the first mode. Thus, the following was the set of comparison functions used

$$\begin{gathered}\phi_1(\xi) = \sqrt{3}\,\xi\;\;, \\ \phi_r(\xi) = \sin(\lambda_r\xi) + \sigma_r \sinh(\lambda_r\xi)\;\;,\;\; for\; r = 2\,,3,\ldots,n\,,\end{gathered} \tag{2.27}$$

where

$$\sigma_r = \frac{\sin(\lambda_r)}{\sinh\,(\lambda_r)}, \tag{2.28}$$

and the characteristic equation for all but the first comparison function is

$$\tan(\lambda_r) - \tanh(\lambda_r) = 0\,. \tag{2.29}$$

The corresponding eigenvalues for the functions in equation (2.26) are

$$\begin{aligned} \lambda_1 &= 0\,, \\ \lambda_r &= 0.25\pi(4r-3)\,, \quad for\ r = 2, 3, \ldots, n\,, \end{aligned} \tag{2.30}$$

where the first eigenvalue corresponds to the rigid body mode. One important aspect of this research project was to observe and analyse how the flexible boundary conditions to be studied would account for the nature of rigid body motion of a pinned-free set-up (see Appendix A for more details). With these questions in mind the model was modified to account for this mode in order to yield appropriate results.

As before, the first three mode shapes of vibration (ϕ's) were plotted for comparison in Maple ®. There is no flow through the pipe; its behaviour is that of a standard beam. These modes will be used as comparison with the models.

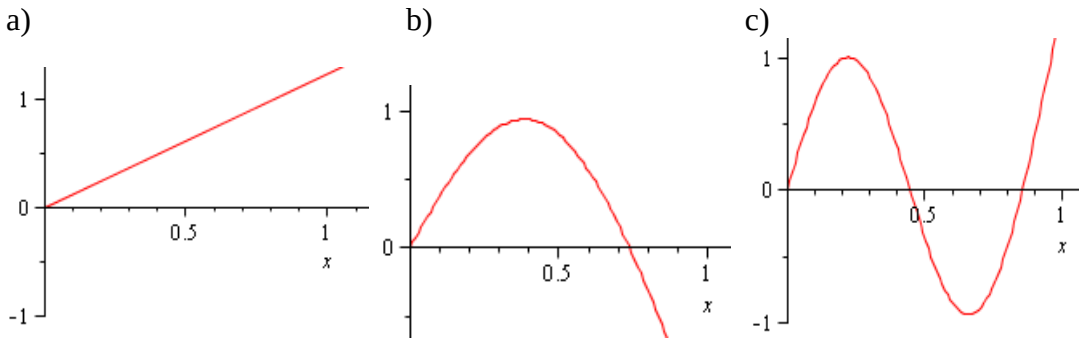

Figure 2.4 - First three modes of vibration for a pinned-free pipe, (a) first mode, (b) second mode, (c) third mode

An observation to be made is how the modes relate to each other for a clamped-free and a pinned-free pipe with no flow. The first mode of vibration for a pinned-free pipe gives a rigid

body mode (in which no bending is present). A cantilevered pipe, on the other hand, has no rigid body modes and instead bends at its first mode (Figure 2.4a). The second and third modes behave in a similar fashion, except at the origin (where the pinned condition allows for rotation).

Applying equation (2.26) into the Galerkin method outlined in section 1.3.2 and then decoupling the system by the process described in section 1.3.3 yields the following results when modelled in Matlab ®

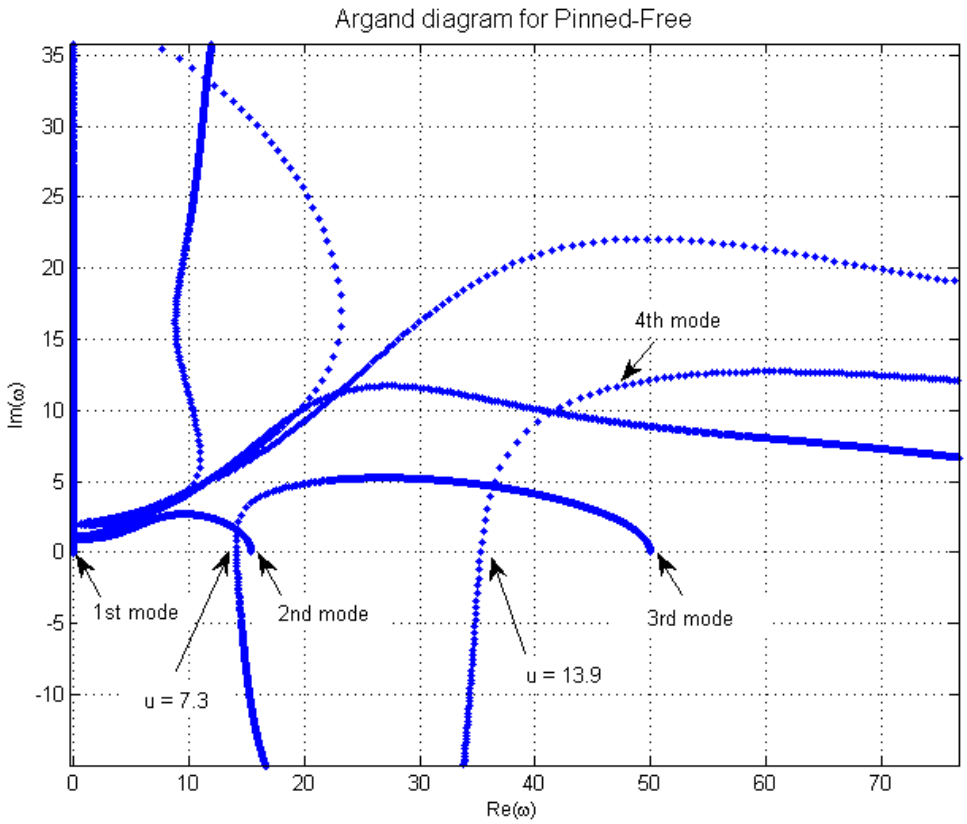

Figure 2.5 - Argand Diagram of a Pinned-Free pipe showing the first three modes for comparison ($\gamma = \alpha = \sigma = 0$) and ($\beta = 0.2$) for $u = 0$ *to* 18

The Argand diagram produced for the standard case of a Pinned-Free beam is shown in Figure 2.5. This graph, which shows the dynamics of the pipe, will be used as a point of reference in the analysis of the pipes with flexible boundary conditions.

Chapter 3
Development and Analysis of Dynamics for Flexible Boundary Conditions

3.1 Dynamics of a Pinned-Free Pipe with a Restraining Spring

To study the dynamic effects of having flexible boundary conditions at the upstream end of a pipe conveying fluid two different scenarios were studied. The first, presented here, consists of a Pinned-Free pipe with a rotational spring of spring constant C at the origin, which will also be referred to as a 'pinned + c'-free pipe. The following diagram better describes the set-up

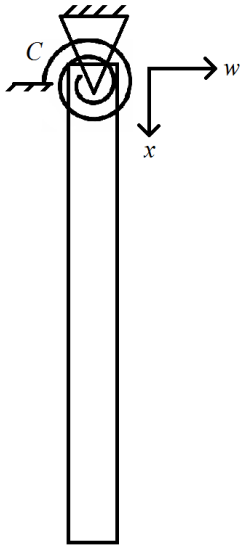

Figure 3.1 – Set-up of a Pinned-Free pipe with a rotational spring at the origin

It is expected that the behaviour of such a pipe will lie in between that of a standard Pinned-Free pipe and a Clamped-Free pipe, depending on the stiffness of the spring attached. A new mathematical model was produced in order to account for the spring in the boundary conditions.

3.1.1 Derivation of the Boundary Conditions

As previously mentioned, a new set of comparison functions is to be derived to create a new model for the system. The boundary conditions, similar to those of a standard Pinned-Free pipe, have to account for the moment produced by the rotational spring, which is dependent on the slope of the pipe at the origin. The nondimensional boundary conditions are the following

$$X(0) = 0\,,\;\; X''(0) - cX'(0) = 0\,,\;\; X''(1) = 0\,,\;\; X'''(1) = 0\,, \tag{3.1}$$

and

$$c = \frac{CL}{EI} \tag{3.2}$$

where C represents the spring stiffness and c its nondimensional counterpart. The solution takes a very complex form due to the boundary conditions presented, unlike a standard Pinned-Free case. A solution for the comparison functions may be reached with the use of the boundary conditions, which will also be dependent on the stiffness of the spring used,

$$\begin{aligned}\varphi_r(\xi) = \; -c\,&\frac{[\sin(\lambda_r) + \sinh(\lambda_r)]\cos\,(\lambda_r\xi)}{2\,\lambda_r \sinh(\lambda_r) + \; c\cos(\lambda_r) + \; c\cosh(\lambda_r)} \\ &+ c\,\frac{[\sin(\lambda_r) + \sinh(\lambda_r)]\cosh\,(\lambda_r\xi)}{2\,\lambda \sinh(\lambda_r) + \; c\cos(\lambda_r) + \; c\cosh(\lambda_r)} + \sin(\lambda_r\xi) \\ &- \frac{[-2\lambda_r \sin(\lambda_r) + c\cos(\lambda_r) + c\cosh(\lambda_r)]\sinh\,(\lambda_r\xi)}{2\lambda \sinh(\lambda_r) + c\cos(\lambda_r) + c\cosh(\lambda_r)}\,.\end{aligned} \tag{3.3}$$

The nondimensional eigenvalues can also be found with the use of the boundary conditions. These may be equated to derive the characteristic equation which yields an infinite amount of eigenvalues

$$\frac{-c{\lambda_r}^3 \sin(\lambda_r)\,(\sin(\lambda_r)+\sinh(\lambda_r))}{2\lambda_r \sinh(\lambda_r)+c\cos(\lambda_r)+c\cosh(\lambda_r)}+\frac{c\lambda^3 \sinh(\lambda_r)\,(\sin(\lambda_r)+\sinh(\lambda_r))}{2\lambda_r \sinh(\lambda_r)+c\cos(\lambda_r)+c\cosh(\lambda_r)}$$
$$-{\lambda_r}^3\cos(\lambda_r)-\frac{(-2\,\lambda_r \sin(\lambda_r)+c\cos(\lambda_r)+c\cosh(\lambda_r))\,{\lambda_r}^3\cosh(\lambda_r)}{2\lambda \sinh(\lambda_r)+c\cos(\lambda_r)+c\cosh(\lambda_r)}=0\,. \tag{3.4}$$

Again, the characteristic equation is also a function of the spring stiffness. With the comparison functions and their corresponding eigenvalues found, a finite approximation may be used in the Galerkin method for the problem. Only the first ten modes of vibration are to be selected and applied through the process as this provides a reliable accuracy level. For the model, different values of the nondimensional spring stiffness, c, will be used to produce the pertinent comparison functions.

3.1.2 Comparison to Standard Cases

Once the model was programmed in Matlab ® (see Appendix D), the first step was to confirm the validity of the model. The first comparison of the model will be compared to a Clamped-Free pipe conveying fluid, as described in section 2.2.1. This case has been studied before (Paidoussis, 1998) and will be used as a benchmark for the flexible model. For the comparison between the cantilevered and flexible models, the large spring constant will be selected to approach a fixed boundary, namely, $c = 10^{12}$. The first three mode shapes of vibration with no flow were plotted in Maple ® to see how each mode compares to the standard cases.

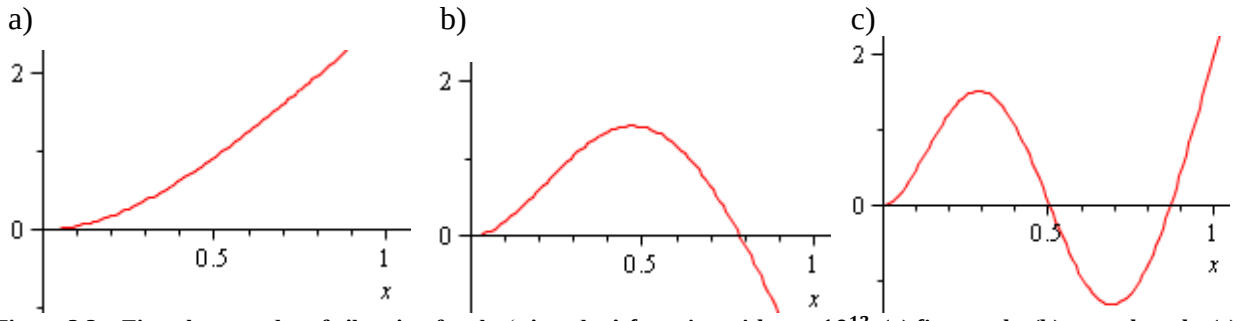

Figure 3.2 – First three modes of vibration for the 'pinned+c'-free pipe with $c = 10^{12}$, (a) first mode, (b) second mode, (c) third mode

The three modes produced are practically identical to those of a regular clamped-free pipe with no flow. Next, fluid flow is added to the model and the results are presented as an Argand diagram.

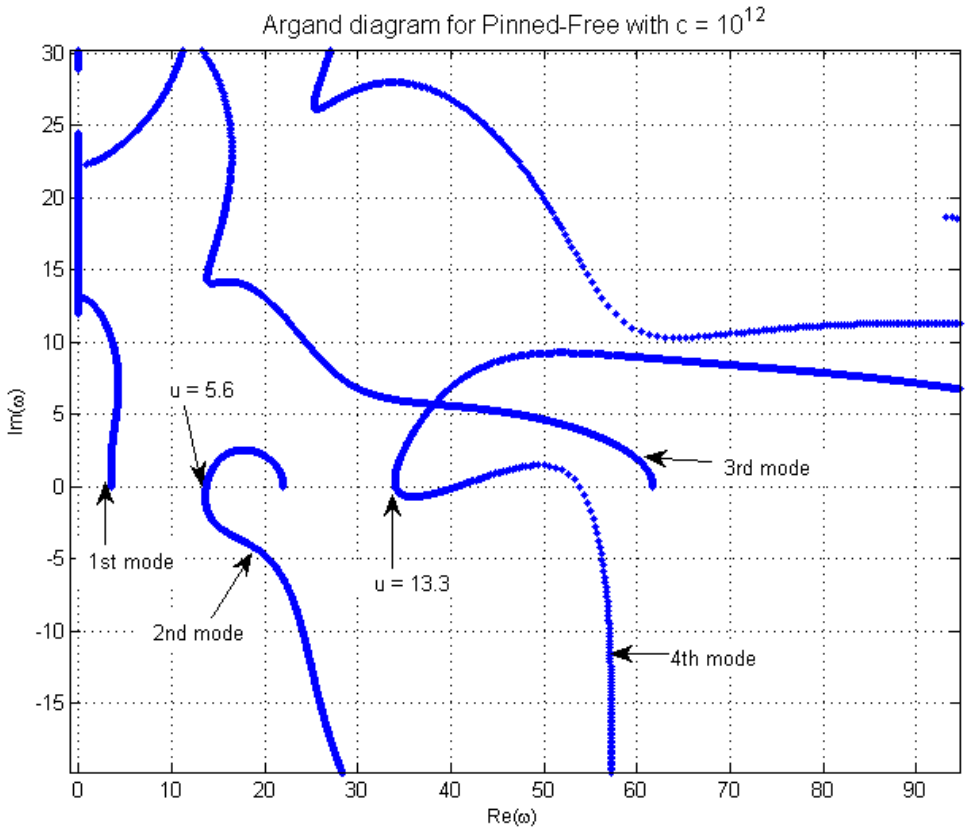

Figure 3.3 – Argand diagram of a Pinned-Free pipe with a rotational spring at the origin showing the first four modes for comparison ($\gamma = \alpha = \sigma = 0$) and ($\beta = 0.2, c = 10^{12}$) for $u = 0$ *to* 18.

The plot shown in Figure 3.3 is identical to that of a standard cantilevered beam presented in Figure 2.3, with the critical velocity for flutter being the same. This suggests that for this limiting case the mathematical model works. To further verify the model, the next step is to observe the opposite limit: setting the spring stiffness to a very low value to approach pinned-free conditions.

In the same fashion that the model approached a cantilevered condition when the spring constant, c, was sufficiently high, the same should be true for a sufficiently low value of c to approach a pinned-free condition. Setting $c = 10^{-9}$ for the stiffness of the spring at the origin produced the modes of vibration in Maple ®, shown in Figure 3.4.

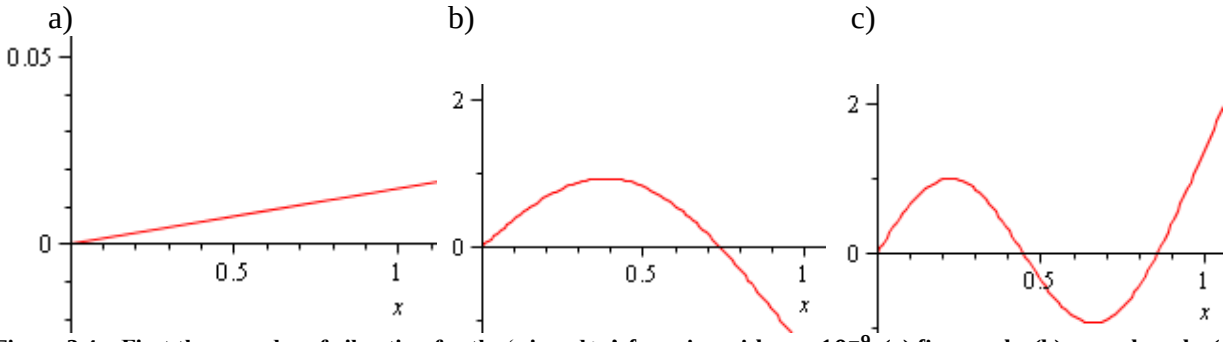

Figure 3.4 – First three modes of vibration for the 'pinned+c'-free pipe with $c = 10^{-9}$, (a) first mode, (b) second mode, (c) third mode

These mode shapes compare directly to those plotted for a classic pinned-free beam. They also show the relationship between the modes, with each mode shape of the pinned-free configuration corresponding directly to its clamped-free counterpart.

Fluid flow was added to the model and the resulting Argand diagram is shown in Figure 3.5.

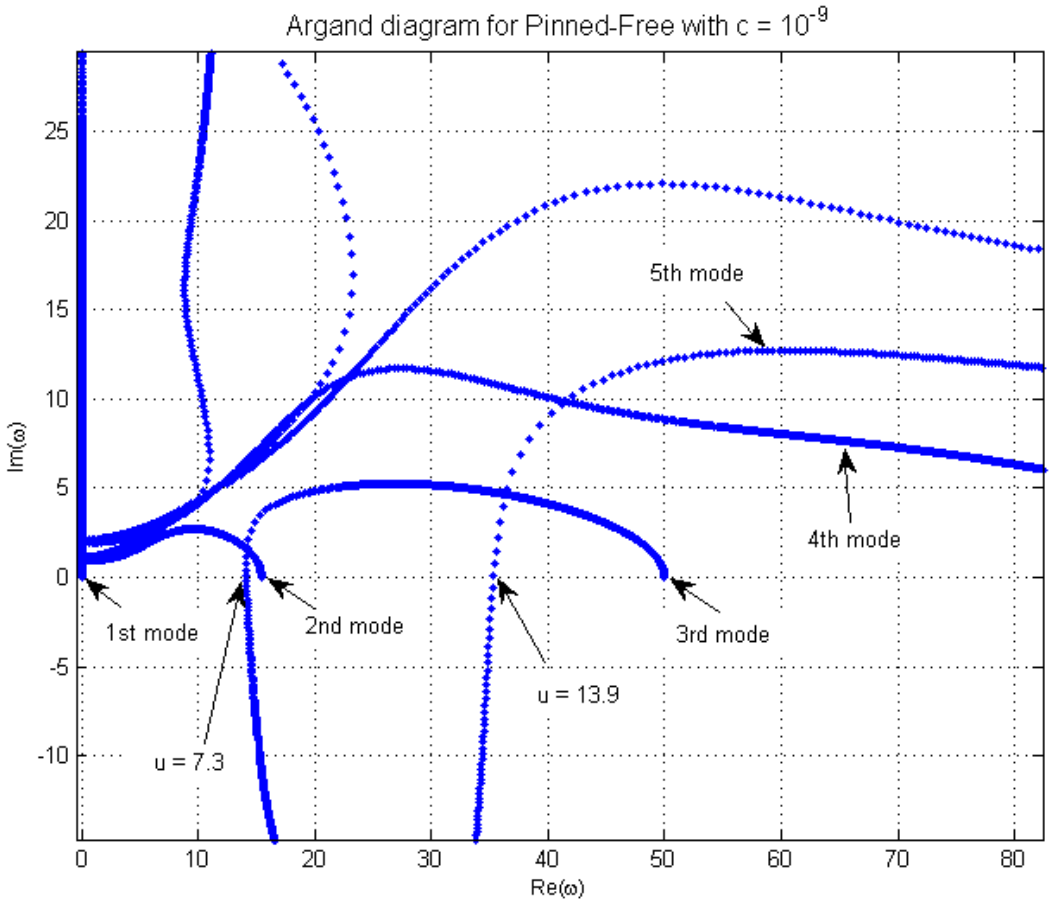

Figure 3.5 - Argand diagram of a Pinned-Free pipe with a rotational spring at the origin showing the first five modes for comparison ($\gamma = \alpha = \sigma = 0$) and ($\beta = 0.2$, $c = 10^{-9}$) for $u = 0$ *to* 18

It is seen that Figure 3.5 shows an accurate approximation to the dynamical behaviour of a Pinned-Free pipe.

Thus, after setting the spring stiffness to both limits it would be safe to assume the mathematical model produced is working properly. After verifying the two limiting cases, the next step is to study the intermediate behaviour of the model between the two classical cases of pinned-free and clamped-free pipes.

3.1.3 Theoretical Results

The purpose of the model is to predict and describe the dynamics of the pipe as the spring stiffness, c, is increased. It is predicted that there will be a smooth transition from the behaviour

of a pinned-free to a clamped-free configuration. Stability is the main focus of the research, and with that said, the most important theoretical result obtained is that of critical flow velocity, u_{cr}.

Before starting the analysis, it is important to make a note about the effect of increasing the mass ratio, β.

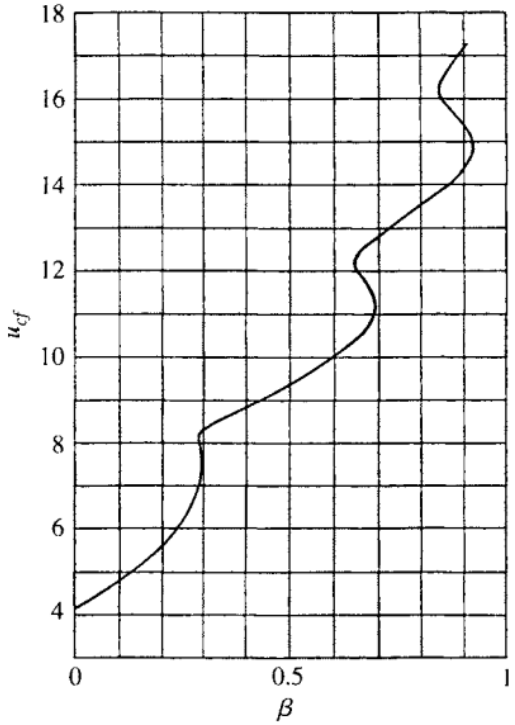

Figure 3.6 – u_{cr} vs β for a standard cantilevered pipe conveying fluid ($\gamma = \sigma = \alpha = 0$) [Gregory & Paidoussis (1966a)]

Figure 3.6 shows the increased stability obtained by increasing the mass ratio, β. Extrapolating from the results obtained by Paidoussis (1998), it is expected that increasing the mass ratio will result in higher critical flow velocities for the cases with flexible boundary conditions as well.

The main focus remains the effect of the spring stiffness on the dynamics, therefore gravity and dissipation have been initially neglected ($\gamma = 0$, $\alpha = 0$, $\sigma = 0$). In order to visualize the transition of the modes of vibration as the pipe was constrained (by increasing the

spring stiffness), the eigenvalues for the first three modes with no flow were tabulated. This shows the smooth evolution from the pinned-free set-up to the clamped-free configuration.

	Pinned-Free	c = 0.001	c = 0.01	c = 0.1	c = 1	c =10	c =100	c = 1000	Clamped-Free
1st mode	0	0.2340	0.4159	0.7358	1.2479	1.7227	1.8568	1.8732	1.8751
2nd mode	3.9266	3.9267	3.9278	3.9385	4.0311	4.3995	4.6497	4.6894	4.6941
3rd mode	7.0686	7.0687	7.0693	7.0756	7.1341	7.4511	7.7827	7.8470	7.8548

Table 3.1 – Transition of modes for the 'pinned+c'-free model from pinned-free to clamped-free with increasing stiffness of c.

Table 3.1 shows how the rigid body mode of a classical pinned-free pipe with no flow smoothly evolves into the first mode of a clamped-free. The other two modes shown also correspond to their clamped-free and pinned-free counterparts. To better display the influence of the flexibility of the boundary conditions, a plot was produced for u_{cr} vs. $\log_{10} c$ for different values of β.

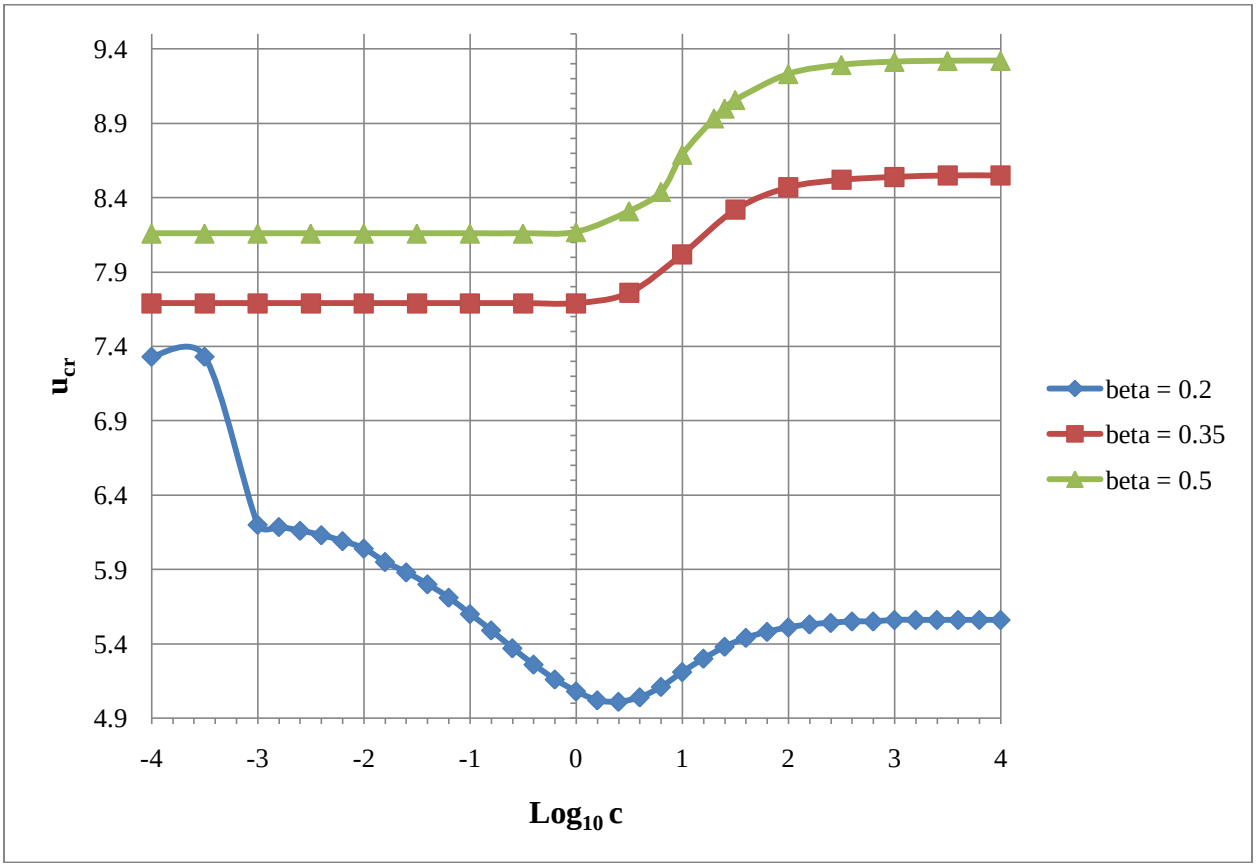

Figure 3.7 – u_{cr} vs. $Log_{10}c$ for a pinned-free pipe with a rotational spring at the origin ($\gamma = \alpha = \sigma = 0$) for several values of β.

Figure 3.7 provides the relationship between the stiffness of the constraining spring and the critical flow velocity for several values of the mass ratio, β. As predicted, the increase in the mass ratio increased the overall stability of the system, regardless of the stiffness of the rotational spring. However, for $\beta = 0.2$, the stiffness has a non-monotonic effect on the dynamics of the pipe. The system loses stability reaching an overall low for critical flow velocity at $c \cong 10^{0.4}$ as stiffness is increased (or a 'critical' stiffness if mathematical terminology may be quoted). The system becomes more stable as it approaches a clamped-free condition, but never regains the stability it had in its pinned-free configuration. This result compares to the previous findings in Chapter 2 as the stiffness approaches the two classical cases ($u_{cr} = 7.3$ for $c = 10^{-4}$, $u_{cr} = 5.6$ for $c = 10^{4}$). For higher mass ratios, stability increases during the transition from a pinned-free to a clamped-free configuration, opposite to that of $\beta = 0.2$. This effect has been studied and described by several authors in the past and will not be discussed further in this thesis [see Paidoussis (1998), Guran & Plaut (1994), Gregory & Paidoussis (1966a)].

A more interesting observation comes from the discontinuity present in Figure 3.7 for $\beta = 0.2$, $\log c = -3$. At first this was assumed to be a numerical error, as all subsequent points present a smooth transition. However, an analysis of each individual Argand diagram for different values of c revealed that the discontinuity is to account for the fact that a clamped-free configuration is divergent (or flutters) through the second mode, while a pinned-free configuration diverges through the third mode. The transition is shown by the following three Argand diagrams for increasing stiffness of the spring.

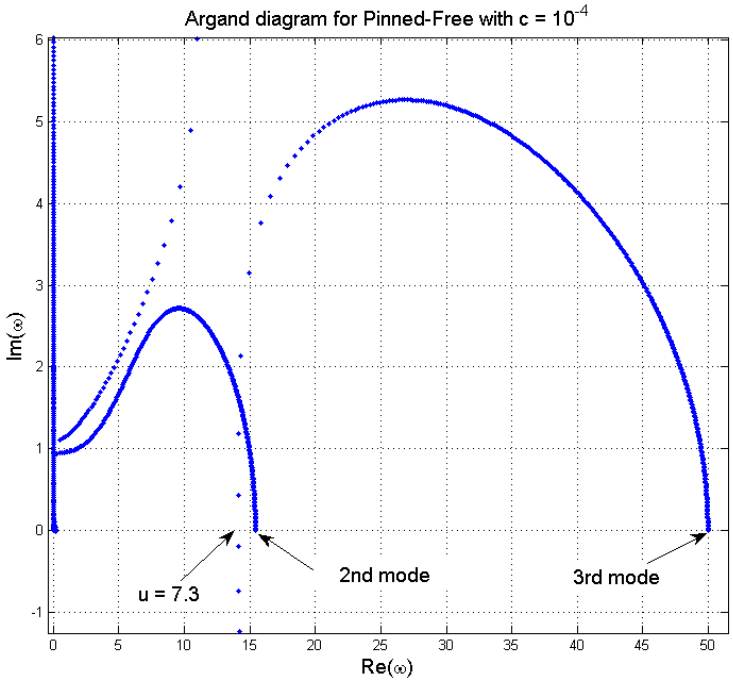
Argand diagram for Pinned-Free with c = 10^-4
Im(ω)
Re(ω)
u = 7.3
2nd mode
3rd mode

a)

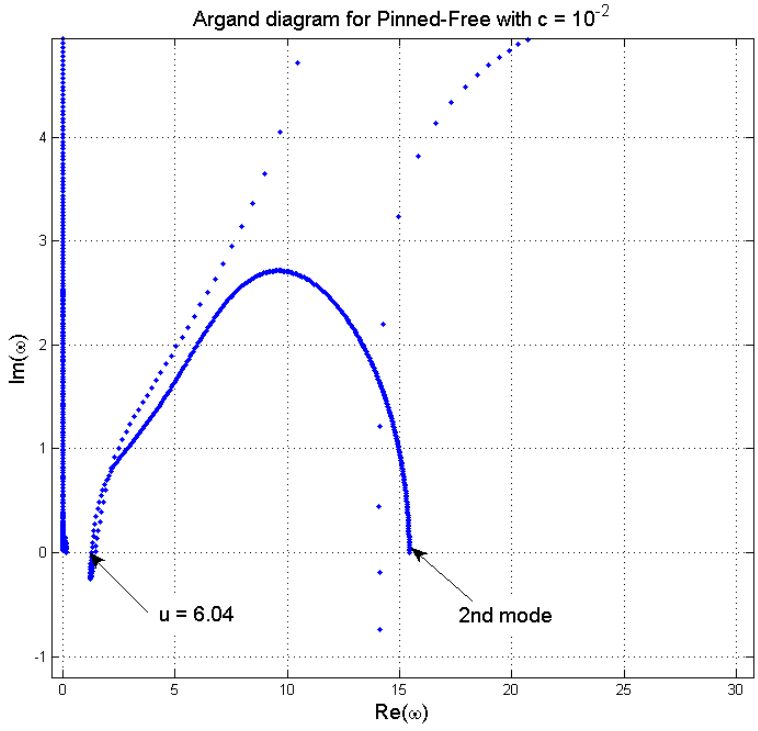
Argand diagram for Pinned-Free with c = 10^-2
Im(ω)
Re(ω)
u = 6.04
2nd mode

b)

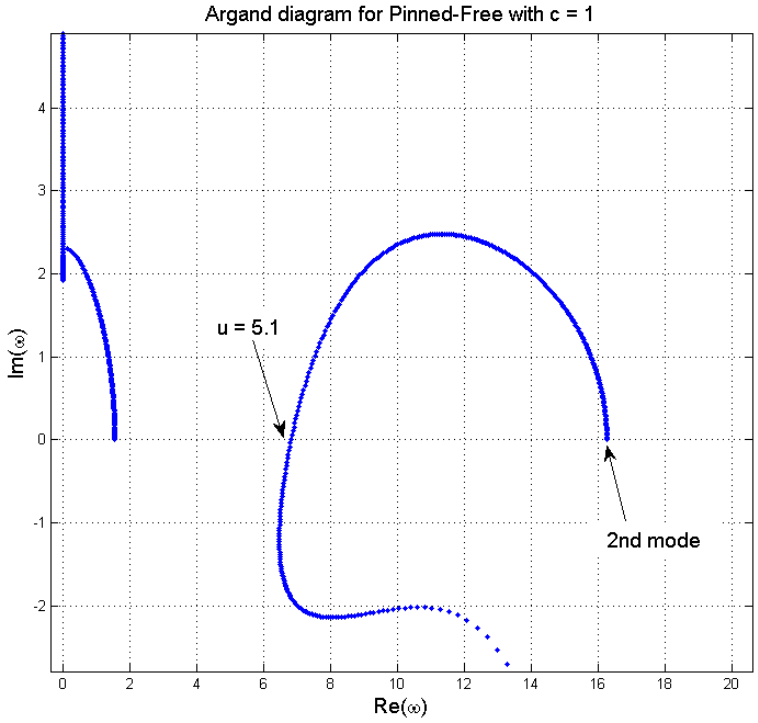

c)

Figure 3.8 – Argand diagrams showing the transition of critical flow velocity between modes for $\beta = 0.2$ ($\gamma = \sigma = \alpha = 0$), (a) approximate pinned-free conditions diverging by 3rd mode ($c = 10^{-4}$), (b) transition between pinned-free and clamped-free with divergence through the 2nd mode ($c = 10^{-2}$), (c) showing the 2nd mode approaching clamped-free conditions

Figure 3.8 provides an explanation for the discontinuity observed in Figure 3.7. A classic pinned-free pipe diverges in the third mode, whereas the classical cantilevered pipe in the second, thereby forcing the model to make a 'jump' at one point. Even though the highest levels of numerical precision were used in the computer program, the method (such as the number of Galerkin modes and the use of a Simpson's rule for the integrals performed) still yielded enough inaccuracy for the model to be unable to pinpoint exactly at what stiffness of c the discontinuity occurs. From the results this is observed to happen in the range between $c = 10^{-5}$ and $c = 10^{-3}$.

The previous case illustrated an idealized system, where gravity and dissipation are neglected. To approach a more realistic system, the parameters of gravity and dissipation are selected based on literature. The values for gravity and viscoelastic damping were chosen from

Paidoussis & Issid (1974) and the value for the viscous damping was obtained by averaging and rounding up two of the values used by Gregory & Paidoussis (1966). The following were the parameters used:

$$\gamma = 10\,,\ \ \alpha = 0.0189\,,\ \ \sigma = 1\,. \tag{3.5}$$

The computer program was run again using the above to produce the plot of Figure 3.9.

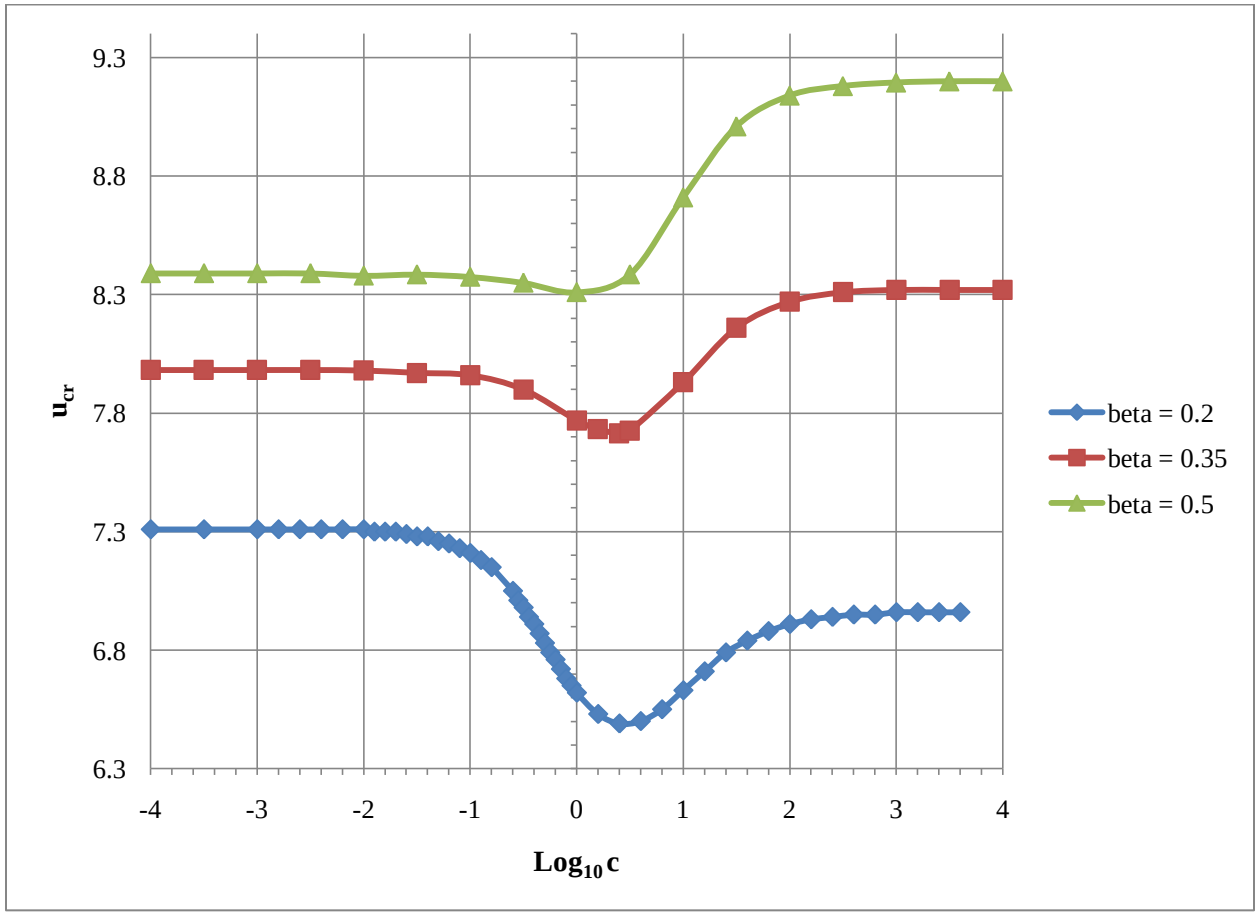

Figure 3.9 – u_{cr} vs. $Log_{10}c$ for a pinned-free pipe with a rotational spring at the origin ($\gamma = 10,\ \alpha = 0.0189,\ \sigma = 1$) for several values of β.

It may be observed in Figure 3.9 that the effect of stiffness is similar to that presented in Figure 3.7. Again, for $\beta = 0.2$ the clamped-pinned configuration has a lower critical velocity than its pinned-free counterpart. This is the opposite of what is obtained for the higher mass ratios presented. As before, the lowest critical flow velocity is given by a stiffness constant of

$u_{cr} = 10^{0.4}$. This suggests that gravity and dissipation has little to no effect on the 'critical' stiffness found (where the lowest u_{cr} is found for an increasing stiffness). This is only a conjecture and not a conclusion. A more in-depth analysis is required to show the relationship between stiffness and the rest of the parameters in question. This, however, will not be studied further as it goes beyond the scope of the research.

3.2 Dynamics of a Free-Free Pipe with Restraining Springs at the Origin

The next model of interest for this project is having a Free-Free pipe with both translational and rotational springs at the origin, in order to give it completely flexible boundary conditions. The model is expected to behave as a fusion of all the three standard cases presented in Section 2.2; this being entirely dependent on the stiffness of the springs. For example, having a very stiff translational spring but a weak rotational one would approach Pinned-Free boundary conditions.

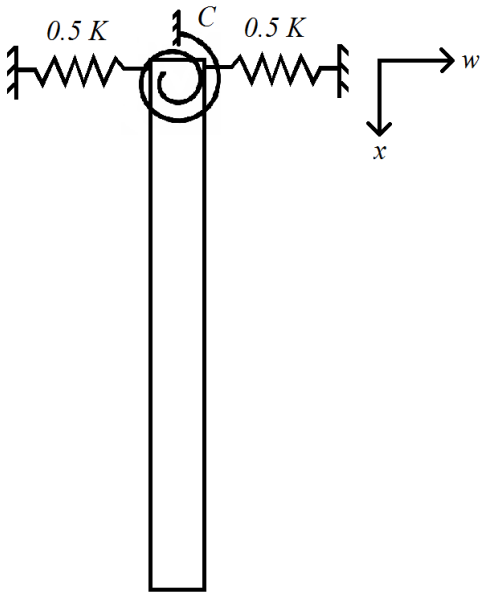

Figure 3.10 - Set-up of a Free-Free pipe with a translational and a rotational spring at the origin

This case will be referred to interchangeably as a 'free + c + k'-free pipe.

3.2.1 Derivation of the Boundary Conditions

The boundary conditions for this problem are the most complex presented thus far due to the two springs. The comparison functions to be derived will be dependent on both the translational spring constant, K, and the rotational spring constant, C. The boundary conditions are the following

$$X''(0) - cX'(0) = 0\,, \quad X'''(0) - kX(0) = 0\,, \quad X''(1) = 0\,, \quad X'''(1) = 0\,, \tag{3.6}$$

and

$$k = \frac{KL^3}{EI}\,, \quad c = \frac{CL}{EI}\,, \tag{3.7}$$

where K is the translational spring constant and k its nondimensional counterpart. Using the method of separation of variables for a simple Euler-Bernoulli beam, as outlined in section 1.3.1, the comparison functions are

$$\begin{aligned}
&\phi_r(\xi) = \mathrm{A}\cos(\lambda_r\xi) + \mathrm{B}\cosh(\lambda_r\xi) + \sin(\lambda_r\xi) + D\sinh(\lambda_r\xi)\,,\\
&A = -\frac{-\lambda^4\sin(\lambda_r) + c\,k\sin(\lambda_r) + \lambda^4\sinh(\lambda_r) + c\,k\sinh(\lambda_r) + 2\,c\,\lambda_r^3\cosh(\lambda_r)}{-\cos(\lambda_r)\;\lambda_r^4 + \cos(\lambda_r)\;c\,k + \cosh(\lambda_r)\,\lambda_r^4 + c\,k\cosh(\lambda_r) + 2\,\lambda_r\,k\sinh(\lambda_r)}\,,\\
&B = -\frac{2\,c\,\lambda_r^3\cos(\lambda_r) - \lambda_r^4\sin(\lambda_r) - c\,k\sin(\lambda_r) + \lambda_r^4\sinh(\lambda_r) - c\,k\sinh(\lambda_r)}{-\lambda_r^4\cos(\lambda_r) + c\,k\cos(\lambda_r) + \lambda_r^4\cosh(\lambda_r) + c\,k\cosh(\lambda_r) + 2\,k\,\lambda_r\sinh(\lambda_r)}\,,\\
&D = -\frac{\lambda_r^4\cos(\lambda_r) + c\,k\cos(\lambda_r) - \lambda^4\cosh(\lambda_r) + c\,k\cosh(\lambda_r) - 2\,k\,\lambda_r\sin(\lambda_r)}{-\lambda_r^4\cos(\lambda_r) + c\,k\cos(\lambda_r) + \lambda_r^4\cosh(\lambda_r) + c\,k\cosh(\lambda_r) + 2\,k\,\lambda_r\sinh(\lambda_r)}.
\end{aligned} \tag{3.8}$$

In turn, the characteristic equation of the system is

$$\begin{aligned}
&\frac{-(-\lambda_r^4\sin(\lambda_r) + c\,k\sin(\lambda_r) + \lambda_r^4\sinh(\lambda_r) + c\,k\sinh(\lambda_r) + 2\,\lambda_r^3\cosh(\lambda_r)\;c)\sin(\lambda_r)\,\lambda_r^3}{-\cos(\lambda_r)\;\lambda_r^4 + \cos(\lambda_r)\;c\,k + \cosh(\lambda_r)\;\lambda_r^4 + \cosh(\lambda_r)\;c\,k + 2\,\lambda_r\sinh(\lambda_r)\;k}\\
&-\frac{(2\,\lambda_r^3\cos(\lambda_r)\;c - \lambda^4\sin(\lambda_r) - c\,k\sin(\lambda_r) + \lambda_r^4\sinh(\lambda_r) - c\,k\sinh(\lambda_r))\sinh(\lambda_r)\,\lambda_r^3}{-\cos(\lambda_r)\;\lambda_r^4 + \cos(\lambda_r)\;c\,k + \cosh(\lambda_r)\;\lambda_r^4 + \cosh(\lambda_r)\;c\,k + 2\,\lambda_r\sinh(\lambda_r)\;k}
\end{aligned} \tag{3.9}$$

$$-\lambda_r^3 \cos(\lambda_r)$$

$$-\frac{(\cos(\lambda_r)\ \lambda^4 + \cos(\lambda_r)\ c\ k - \cosh(\lambda_r)\ \lambda_r^4 + \cosh(\lambda_r)\ c\ k - 2\ \lambda_r \sin(\lambda_r)\ k)\cosh(\lambda_r)\ \lambda_r^3}{-\cos(\lambda_r)\ \lambda_r^4 + \cos(\lambda_r)\ c\ k + \cosh(\lambda_r)\ \lambda_r^4 + \cosh(\lambda_r)\ c\ k + 2\ \lambda_r \sinh(\lambda_r)\ k}$$

$$= 0\ .$$

Equation (3.9) may be solved analytically using Maple ® to yield an infinite number of eigenvalues for each of the modes given by the comparison functions. Again, all eigenvalues found are dependent on the magnitude of the stiffness selected for each spring.

3.2.2 Comparison to Standard Cases

As with the previous model, the first step is to verify the validity of the model by comparing it to the three standard cases presented in Section 2.2. The first is a comparison of the set-up of a cantilevered pipe conveying fluid. Firstly, the modes of vibration with no flow are to be plotted using Maple ®.

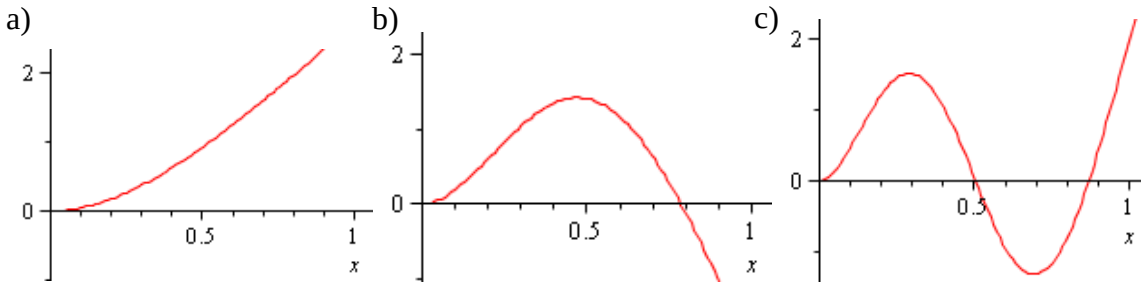

Figure 3.11 – First three modes of vibration for the 'free+c+k'-free pipe with $c = 10^{12}$ and $k = 10^{12}$, (a) first mode, (b) second mode, (c) third mode

The modes plotted in Figure 3.11 replicate those of a classic cantilevered beam. This shows that the correct comparison functions and eigenvalues were derived.

Next, flow through the pipe is considered and the Argand diagram produced, which shows the dynamical behaviour of the pipe. The plot is shown in Figure 3.12.

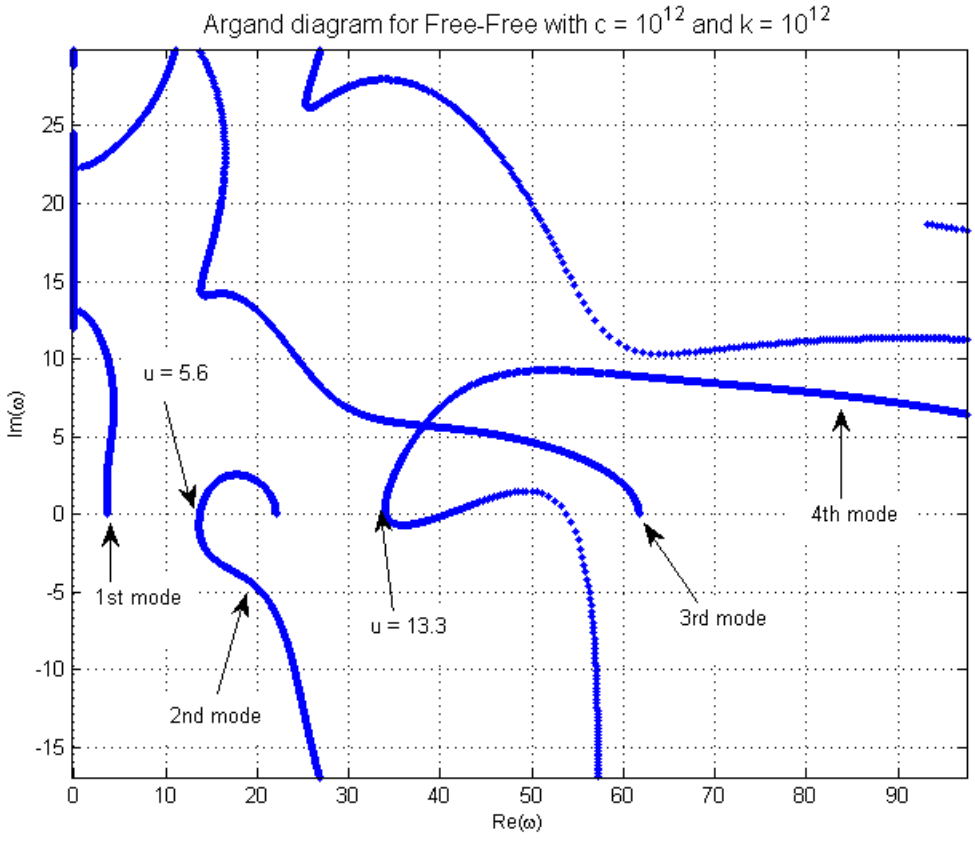

Figure 3.12 - Argand diagram of the Free-Free pipe with a translational and a rotational spring at the origin showing the first four modes for comparison ($\gamma = \alpha = \sigma = 0$) and ($\beta = 0.2, k = 10^{12}, c = 10^{12}$) for $u = 0$ *to* 18.

To approach the boundary condition of a cantilevered the two spring constants are set to $k = 10^{12}$ and $c = 10^{12}$. This is successfully achieved, as seen in Figure 3.12, as the Argand diagram is identical to that of a clamped-free configuration, showing as well the same critical flow velocities for flutter.

As with the previous model, this one will now be compared to a classic pinned-free pipe. The first step is to compare the modes of vibration without flow to ensure the correct derivation of the comparison functions and eigenvalues of the system. The results are shown in Figure 3.13.

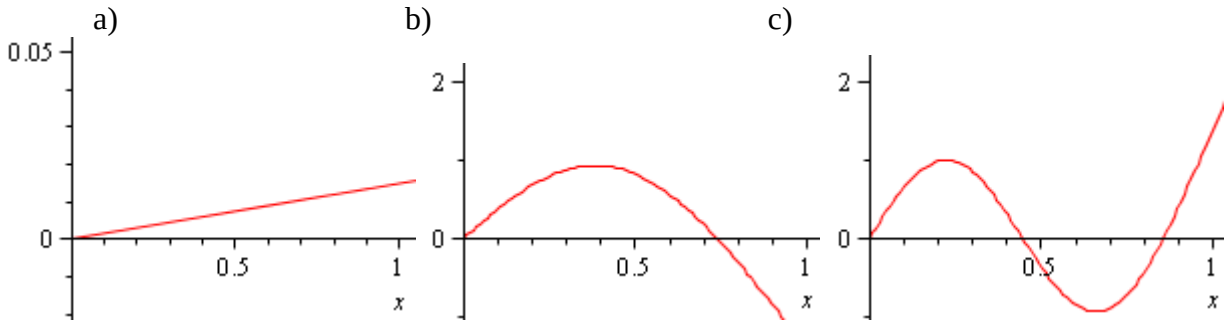

Figure 3.13 – First three modes of vibration for the 'free+c+k'-free pipe with $c = 10^{-9}$ and $k = 10^{12}$, (a) first mode, (b) second mode, (c) third mode

With the results showing that the comparison functions were properly derived, all that remains is to consider the dynamics after adding fluid flow to the system. The resultant Argand diagram is shown in Figure 3.14.

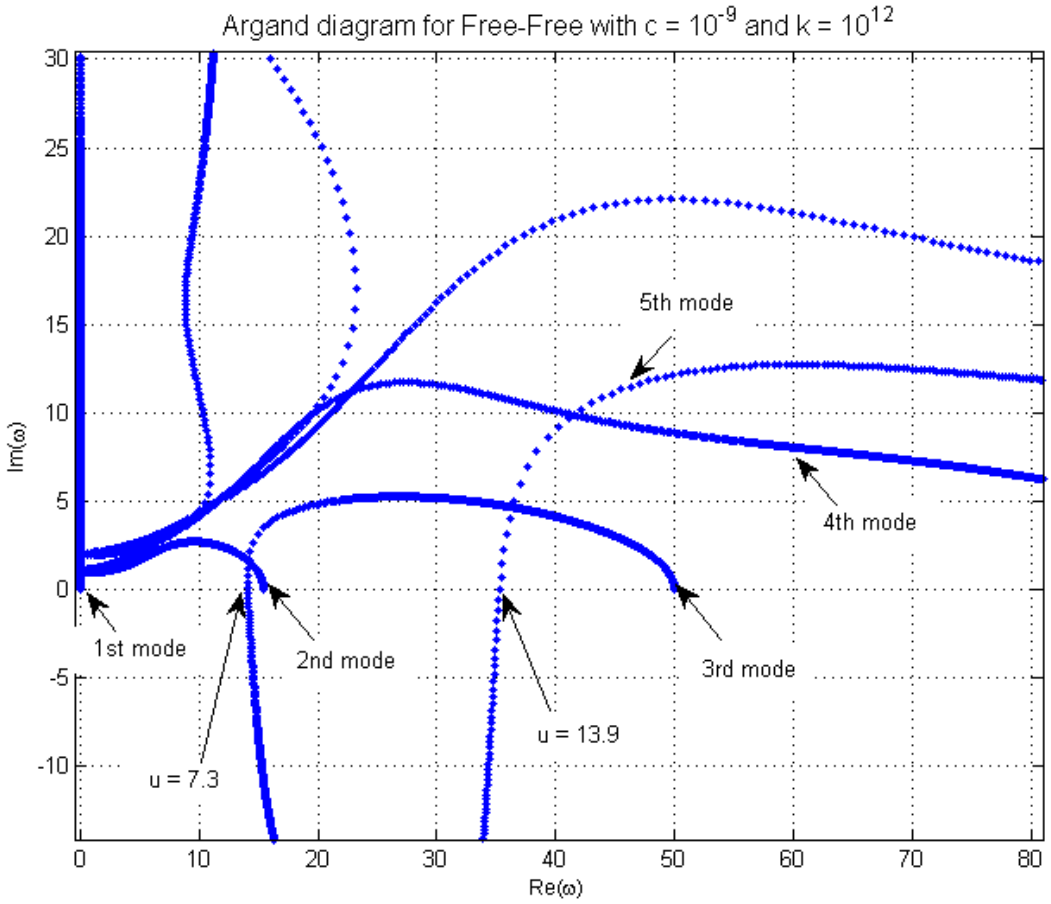

Figure 3.14 – Argand diagram of the Free-Free pipe with a translational and a rotational spring at the origin showing the first four modes for comparison ($\boldsymbol{\gamma = \alpha = \sigma = 0}$) and ($\boldsymbol{\beta = 0.2}$, $\boldsymbol{k = 10^{12}}$, $\boldsymbol{c = 10^{-9}}$) for $\boldsymbol{u = 0}$ *to* 18.

After setting the stiffness constants of the translational and rotational springs to $k = 10^{12}$ and $c = 10^{-9}$ respectively, it may observed that Figure 3.14 accurately reproduces the dynamic behaviour of a pipe with standard pinned-free boundary conditions.

The previous comparison to standard cases shows that the limits of the model are very accurate and precise, leading to evidence that the model will yield a valid solution for all intermediate scenarios of the boundary conditions.

3.2.3 Theoretical Results

Unlike the previous model studied, for this one all the results were plotted only for one value of the mass ratio, namely $\beta = 0.2$. This is due to the increase in the number of variables in the system, as now the results are displayed as plots for several values of the translational spring stiffness, k. Based on theory, however, the conjecture is made that stability will increase with an increasing mass ratio.

To better observe the effect of increasing stiffness on the overall stability of the pipe the following plot shown in Figure 3.15 was produced.

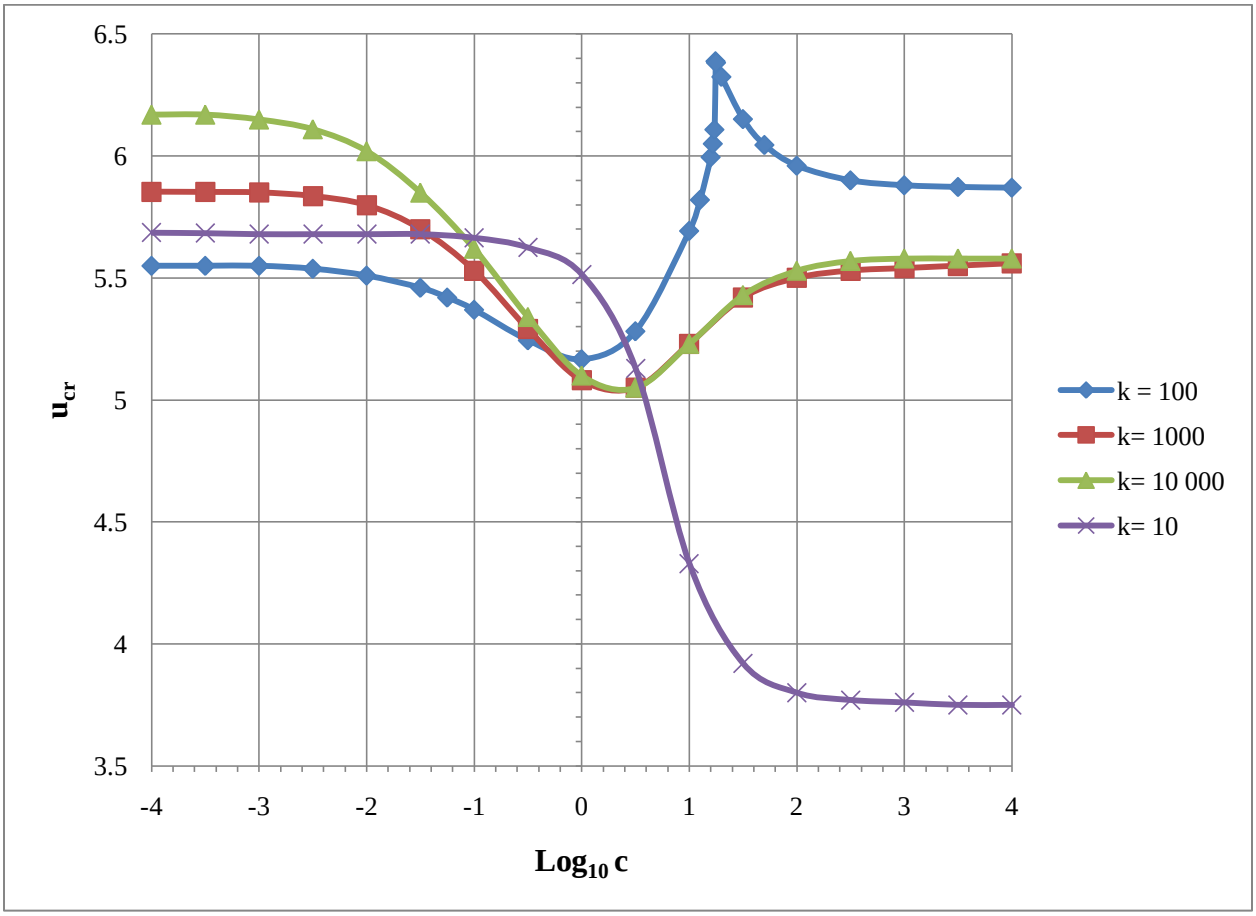

Figure 3.15 – u_{cr} vs. $Log_{10}c$ for a pinned-free pipe with a rotational spring at the origin ($\gamma = \alpha = \sigma = 0$) for several values of k

The results in Figure 3.15 illustrate how the critical fluid flow velocity varies as the rotational spring stiffness is increased. The plot was produced for several values of the translational spring stiffness. The results show several interesting facets of behaviour for the different values of k.

Starting with the dynamics described for both $k = 10^3$ and $k = 10^4$, the results come as no surprise. They show a similar pattern to that of the previous model with a pinned end (the pin being equivalent to a stiffness of $k = \infty$). It is interesting to observe, however, that as the stiffness of k is decreased from 10^4 to 10^3 the overall stability decreases for all values of c.

For the translational stiffness of $k = 100$ the results were unexpected, with a peak being observed at $c = 10^{1.245}$. A more in depth analysis of the individual Argand diagrams around that point was therefore undertaken.

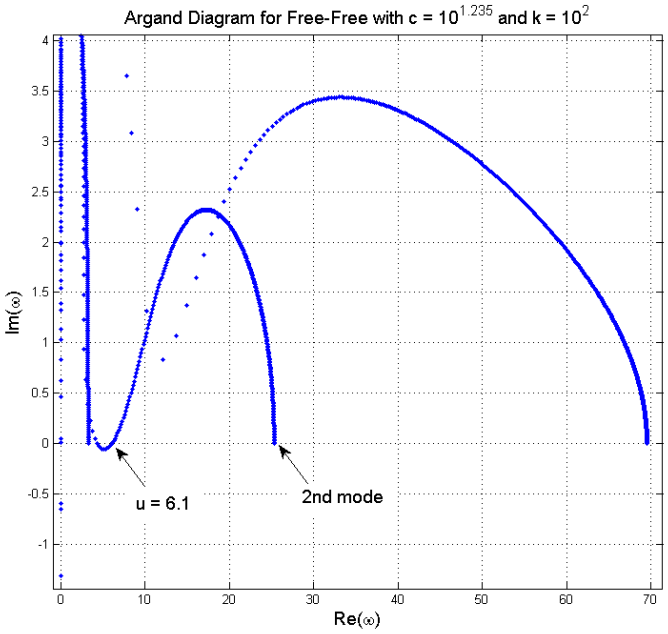

a)

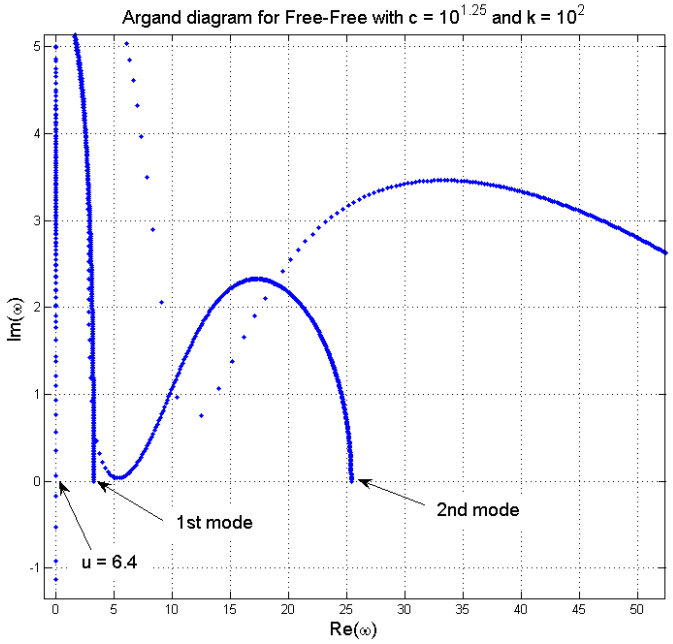

b)

Figure 3.16 - Argand diagrams showing the transition of critical flow velocity between modes for $\beta = 0.2$ ($\gamma = \sigma = \alpha = 0$), showing (a) divergence by 2nd mode ($c = 10^{1.235}$), and (b) divergence by 1st mode ($c = 10^{-1.25}$)

Figure 3.16 shows two Argand diagrams which give an explanation for the sudden peak reached for $k = 100$ in Figure 3.15. There is a shift in the mode of divergence from the second mode (for values of $c < 1.245$) to the first mode (for values of $c > 1.245$). However, these results reveal a fundamental error in the model. The instability through the first mode presented is a static divergence, or buckling, which should be impossible for a pipe with an unconstrained downstream end. The explanation for this error was found by looking at the eigenvalues of vibration (λ's). A classic free-free pipe with no flow has two rigid body modes. It has a rotational and a translational normal mode, with the two corresponding eigenvalues equal to zero. A closer look at the eigenvalues given by the model led to the results tabulated in Table 3.2.

	Model ($k = 10^{-9},\ c = 10^{-9}$)
1st mode	0.5515
2nd mode	4.7320
3rd mode	7.8544

Table 3.2 – Eigenvalues of vibration for the first three modes with no flow for the 'free + c + k'-free model at the limiting case approaching a standard free-free pipe

The eigenvalues presented in Table 3.2 demonstrate that the model fails to account for the two rigid body modes found in a classic free-free configuration. The case could not be analysed in detail as literature for a classic free-free pipe is not readily available. This is partially due to the unrealistic applicability of this configuration for a pipe conveying fluid.

Nevertheless, another set of results was produced to demonstrate the effects of gravity and dissipation in the model. The same assumptions as those in Section 3.1 were made for the parameters, selecting them to be

$$\gamma = 10\,,\ \ \alpha = 0.0189\,,\ \ \sigma = 1\,. \tag{3.10}$$

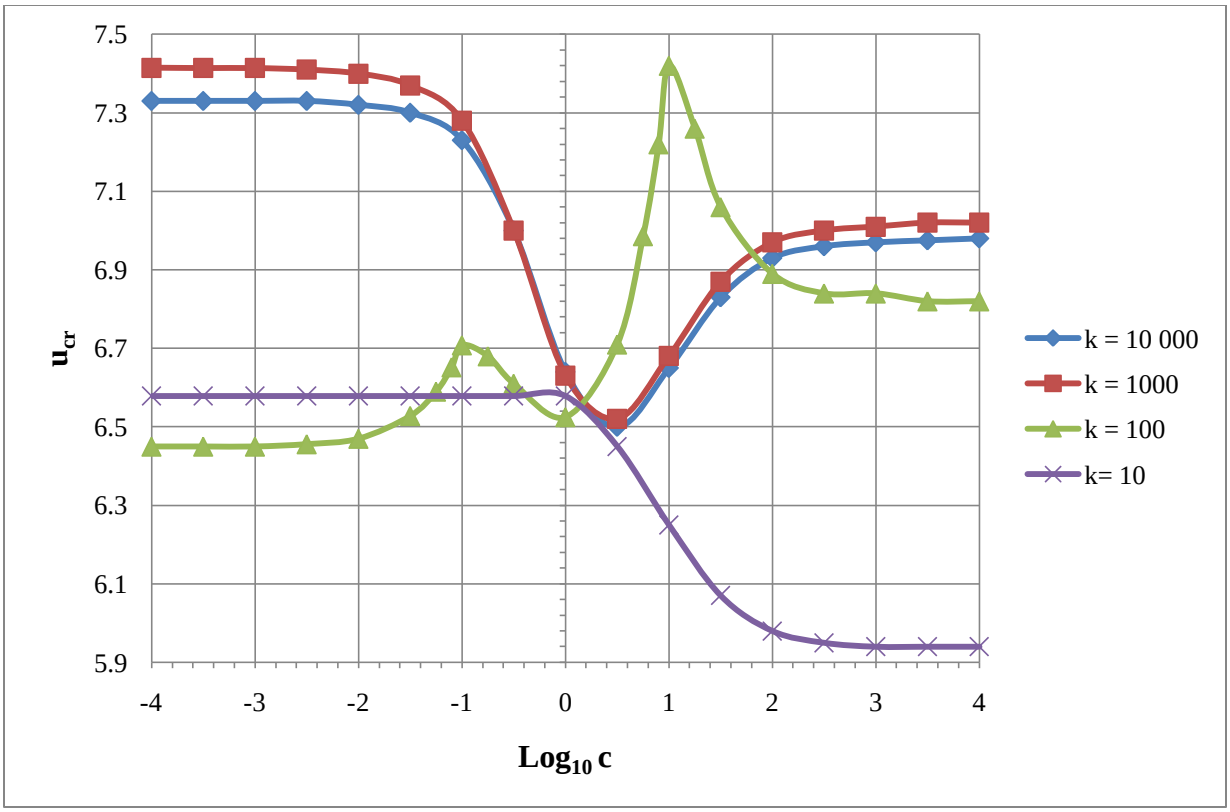

Figure 3.17 – u_{cr} vs. $Log_{10}c$ for a pinned-free pipe with a rotational spring at the origin ($\gamma = 10, \alpha = 0.0189, \sigma = 1$) for several values of k

The results showed a similar behaviour as the one identified in Figure 3.15. Again, this is evidence which suggests that the addition of gravity and dissipation does not influence the behaviour described by increasing stiffness. It only increases overall stability of the model. However, the plot for $k = 100$ shows two peaks instead of one. A closer look at the corresponding Argand diagrams revealed that once more there was buckling present, reinforcing the statement that the model did, in fact, collapse for low values of k as the model cannot account for two rigid body modes. Therefore, it is deemed that this model was produced with a limit to the value of k for which it remains valid. Moreover, an exact value for the limit translational stiffness could not be determined precisely due to the non-existence of comparison models from literature. It is deemed that this model is not infallible and more work is required for a proper development of a free-free beam constrained only by springs.

Chapter 4
Experimental Set-up and Results

4.1 Experimental Apparatus

The apparatus used for the experiment is an already existing apparatus (Jamin, 2010), which had to be repaired as it had suffered considerable damage, as a result of renovations in the Macdonald Engineering Building at McGill University. The apparatus consists of a stainless steel vessel where the experiments are to be conducted, connected to a reservoir where water is kept. There is much flexibility when deciding the direction of the flow through the vessel. The adaptability is possible thanks to the design of the apparatus, which has many sources and sinks. These can be modified thanks to a set of removable tubes in order to control the flow coming from the two pumps. For the purpose of this research, only one pump is required as there is only flow in discharge or aspiration through the pipe.

4.1.1 Repair and Modification of the Apparatus

The apparatus used for the experiments of this thesis was designed by Jamin (2010), which consists of a stainless steel vessel through which water is pumped. The vessel itself can hold a clamped pipe, and water can be discharged and aspirated either through the clamped pipe or through an annulus around it. Figure 4.1 shows the complete apparatus used during the experiment.

Figure 4.1 – The experimental apparatus used [designed and built by Jamin (2010)]

The apparatus was damaged and parts were misplaced or lost since it was last used. A brass fitting and its corresponding hose were missing from the top of the apparatus. The two components had to be replaced and reattached. Next, the design of the apparatus was modified by adding a new release valve at the top to prevent air pressure build inside. The top plate was machined to allow for the new valve. The previous valve was located at the mid-section instead of the top, meaning that air would remain trapped inside the vessel during operation. The new valve allows for most of the air to be released.

The flow straighteners at the top and bottom of the apparatus were also missing. Two sheets of perforated plastic and a schedule 80, PVC, unthreaded, 8 inch diameter pipe were ordered (from *McMaster-Carr*) to later manufacture the missing flow straighteners. From the perforated sheets, two 18 inch diameter discs and two 7.5 inch diameter discs were manufactured. The former were then tightly attached to the bottom of the vessel. The two smaller discs were then fitted into machined segments of the schedule 80, PVC pipe. These two pairs of

discs serve as flow straighteners for both top and bottom of the machine. Having straight flow is important in the experiment to avoid apparent (not real) instabilities from occurring due to turbulence in the flow.

Finally, the front window of the vessel had also been damaged and had a fissure propagating around one of the bolts. To prevent the window from shattering it was reinforced by the use of two thin sheets of Lexan ® plastic. These are very flexible yet strong, thus providing a good reinforcement to the window.

After the repairs were made the apparatus was finally operational. All that was required now was the installation of a drain system and the attachment of a magnetic flow meter. The next step to take was to cast and prepare the pipes to be used during the experiment.

4.1.2 Pipe Casting and Pipe Properties

The pipes used during the tests conducted were cast specifically for this experiment. This was to ensure the quality and consistency of the pipes used, as the pipes must be perfectly straight and in good condition. A pipe casting apparatus, designed by Paidoussis (1998, Appendix D), was cleaned and mended for the purpose. The steps taken to fabricate each of the pipes are described carefully in Appendix B. Two white, silicone rubber pipes were cast for the experiment, with different flexural rigidities.

To allow for a fair comparison between the theoretical results and experimental ones, the flexural and viscoelastic properties of the pipes had to be carefully measured. The natural frequencies of the first three modes of vibration were obtained for each pipe by exciting the pipes to arbitrary frequencies and then allowing them to decay. Natural frequencies are predominant when there is no forcing frequency. With the first three natural frequencies, the pipes were then

excited to each individual frequency and then their motion was allowed to decay freely in order to measure the logarithmic decrement accurately. With the natural frequencies, and their corresponding logarithmic decrements, the flexural rigidity (EI) and viscoelastic dissipation (c^*) were calculated by extrapolation from tabulated data from Paidoussis & des Trois Maisons (1969). A detailed explanation of the procedure used to find these two properties can be found in Appendix C. The remaining properties of the pipes to record were mass, diameters, and length, all of which are easy to determine. The properties found for both pipes are listed in Tables 4.1.

	Pipe 1	Pipe 2
Mass per unit length (m) (kg/m)	0.1392	0.1360
Added mass per unit length (m_f) (kg/m)	0.1899	0.1973
Fluid mass per unit length (M) (kg/m)	0.07118	0.07118
Length (L) (m)	0.4410	0.4250
Inner diameter (m)	0.00952	0.00952
Outer diameter (m)	0.01585	0.01555
Flexural rigidity (EI) (N.m^2)	4.904e-4	4.199e-4

Table 4-1 – Casted pipe properties

From Table 4.1 the pipe properties were made nondimensional in order to compare to the models previously made. The viscoelastic dissipation found from Paidoussis & des Trois Maisons (1969) was already a nondimensional property and will be included in Table 4.2. Determining a value for dissipation to the surrounding fluid, σ, was experimentally very demanding and could not be determined for the pipes cast. However, approximate values for dissipation in water were obtained from the literature (Paidoussis, 1998) and are given in Table 4.2.

	Pipe 1	Pipe 2
Mass ratio (β)	0.1744	0.1793
Gravity parameter (γ)	238.74	243.91
Viscoelastic dissipation (α)	0.02730	0.02238
Dissipation to fluid (σ)	0.018	0.018

Table 4-2 – Nondimensional parameters for casted pipes

Once the parameters were determined the pipes were tested in the vessel, one at a time.

4.2 Experimental Set-up

Due to the difficulty of replicating flexible boundary conditions with a measurable stiffness the set-up used was that of a clamped-free pipe. The pipes were attached to a brass fitting and held firmly in place. The vessel is then filled completely with water, ensuring that all air has been released to avoid having a pressure differential. This is achieved by releasing the air from the new air release valve.

The equipment used to determine the frequency of vibration of the pipe was an Optron ® system. It operates by using a light interface, whereby it selects the point with the highest light intensity and tracks its motion. A bright light source was used to shine light on the white pipes. The Optron ® system is then calibrated and used to provide input to LabVIEW ®, computer software which simulates instrumentation hardware. LabVIEW ® allows the user to filter, display and record the output from the Optron ® system. This can then be processed in Matlab ® to identify the frequency of interest. The process is very similar to that described in Appendix C to obtain the pipe properties.

4.3 Experimental Results

With the vessel ready and the pipe in place, the flow velocity was increased very slowly to avoid disturbing the pipe due to fluid flow acceleration and turbulence. Obtaining the experimental data proved to be very troublesome for the Optron ® due to light refraction through the water.

Other problems arose due to the flexibility of the pipe cast. The material used did not have the required stiffness for this particular experiment. Their high flexibility meant that low

flow velocities would bend the pipes, or ‘kink’ them to one side. Experimentally, it was of great importance for the pipes to remain straight up to the critical point. Having the pipe bent meant that the dynamics of the pipe were changed beyond agreement with the model produced. This made predictions produced from the clamped-free model (section 2.2.1) not applicable to the experiment. The apparatus was drained and the pipe straightened to correct this. However, the problem was recurrent and it happened in every test run. Therefore, the experimental results were qualitative rather than quantitative.

Increasing the flow slowly illustrated how instabilities arise naturally. After a given threshold, motion would suddenly be detected in the pipe, with oscillations of a very low frequency and amplitude. However, measurable increments in flow velocity through the pipe of approximately $u \cong 0.05$ had a sizeable effect on both the frequency of oscillation and its amplitude. After a small increase in velocity the pipe could be observed to be in full flutter, going from steady planar motion to chaotic three-dimensional motion, until it eventually reached a constant rotational behaviour.

The experiment illustrated the slow evolution of instabilities as fluid flow increases through the pipe. All the stages of flutter were also observed during the experiment, giving a much better understanding of the theory previously described in the thesis.

Future experiments should be conducted in order to quantitatively verify the theoretical results produced by the classic models. Addition of measurable flexible boundary conditions to the experimental set-up would also add a new dimension to the experiment as it would confirm or deny, empirically, the findings predicted by the theoretical models developed.

Chapter 5
Conclusion

The overall objective of the thesis was to better understand the influence of flexible boundary conditions in the stability of pipes conveying fluid. This was achieved by creating two mathematical models with flexible conditions constraining the motion of one end, while having a 'free' condition at the other. The models were then verified by theory and literature, comparing them to classical configurations of pipes (clamped-free and pinned-free). Subsequently, these models were used to predict the dynamical behaviour of a pipe conveying fluid for different values of stiffness. The experiment provided valuable qualitative information to better understand the development of self-excited instabilities in the system. It also allowed the author to observe the 'mixed' modes of vibration during flutter.

5.1 Theoretical Predictions

The thesis focus was mainly theoretical and most of the time and effort was invested in the derivation of the two flexible models in order to analytically observe the effect of flexibility in the pipe conveying fluid dynamics.

5.1.1 Stability of a Pinned-free Pipe with a Rotational Spring at the Origin

The first model produced, a pinned-free pipe with a rotational spring at the origin, was to behave as an intermediate support between the two classic cases of a pinned-free and clamped-free pipe. In the boundary conditions the spring was accounted for during the derivation of the comparison functions, including the stiffness in the moment equation at the origin. The comparison functions derived were functions of both the longitudinal coordinate (ξ) and the

spring stiffness (c). The mode shapes of vibration would give the correct geometrical and natural boundaries for any given stiffness. These were then used with the Galerkin method to find a solution.

The resulting mathematical model correctly emulated the normal modes of vibration (with no fluid flow) and the dynamics of a clamped-free pipe conveying fluid for large values of c and of a pinned-free pipe for low values of c. This data suggests that the model is appropriate.

The model was then used to produce predictions about the stability of the pipe in relation to increasing spring stiffness. The stability was judged based on the critical flow velocity of the pipe, at which the pipe becomes self-excited. The results indicated that, starting from an approximate pinned-free configuration (low value of c), increasing stiffness decreased the stability of the pipe. The pipe would reach an overall minimum at an intermediate point, after which stability increased and converged to the value for stability of a standard clamped-free pipe. The destabilizing effect of increasing stiffness was shown to be independent of mass, gravity and dissipation, although the actual stiffness for minimum stability (or 'critical stiffness') may change when the aforementioned parameters are varied.

The correct development of the model also allows for future research. The model may be used to study the relationship of stiffness versus other parameters, such as gravity and dissipation, to better understand how the exact value of critical stiffness changes with these parameters.

5.1.2 Stability of a Free-free Pipe with Restricting Springs at the Origin

The development of this particular (and peculiar) model proved to be more challenging than expected. The springs, both translational and rotational, were included in the boundary conditions in the force and moment equations at the origin. The derivation that followed made the comparison functions a function of ξ, k, and c.

The mathematical model developed was first tested without flow to observe and compare the mode shapes produced. After successfully comparing the model to a standard pinned-free pipe and a standard clamped-free pipe, flow was then added and the results compared again. The second test was successful. However, a problem arose for low values of k. The pipe was never compared against a standard free-free pipe.

A classic free-free pipe has two rigid body modes, both with a corresponding zero eigenvalue. However, the model developed will only emulate one of them, failing to account for the other. Thus, as decreasing values for the translational stiffness are used, results suggest that the model collapses as they indicate the pipe conveying fluid is diverging statically, not dynamically, which should not be possible for a pipe with an unconstrained end.

5.2 Experimental Findings

The experiment performed was useful in illustrating the development and overall effect of flutter in a cantilevered pipe conveying fluid. Preparing all the equipment for the experiment required several steps: repairing the apparatus, casting the pipes (see Appendix B), and determining the pipe properties (see Appendix C).

Obtaining experimental results, however, proved to be more challenging than expected. The Optron ® system was unable to pick a reliable interface of light and all subsequent results

obtained were defective. Nevertheless, the experiment served its purpose from a qualitative point of view in order to better understand how flutter appears and evolves in a cantilevered pipe.

The pipe remains completely static as flow is increased up to a critical point when a small step increase results in a very minute amplitude and frequency of vibration. However, with passing time, the amplitude increases. Further increases in the fluid flow velocity results in a higher frequency and amplitude. Oscillations evolve from sinusoidal and planar to chaotic and three-dimensional rotary.

5.3 Future Work

From the conclusions reached before, it is important to delineate what possible research paths may follow. Starting with the model derived for the pinned-free beam with a rotational spring at the origin, it would be possible to use the existing model to investigate other instances regarding the dynamics of a pipe with flexible boundary conditions. The relationship of stiffness to other parameters, such as gravity or dissipation, may be explored using the existing model. Using the model to study aspiration with flexible boundary conditions is another possibility. This may be achieved by correctly expanding the model to account for the terms relating to aspiration. The same is possible for pipes in axial flow conveying fluid.

Next, the second model derived, although not successfully, may serve as a stepping stone for the correct development of such a model. Having the possibility of a fully flexible model would allow for the theoretical investigation of many interesting pipe dynamics. The physics behind such a model would not only yield applicable models but also very interesting fundamental results regarding pipes conveying fluid. The improvement required is to correctly account for both translational and rotational rigid body modes.

Finally, the experimental aspect of this thesis may be greatly improved by obtaining not only qualitative results but also by collecting quantitative data. This would allow for a direct numerical comparison with the theoretical predictions from the models. Another dimension that could be added is the inclusion of flexible boundary conditions to the experiment. If a set of measurable boundary conditions is developed to fit in the apparatus then the predictions generated by the mathematical models may be tested empirically in order to fully verify the results given. Stiffer pipes should be cast and used for the experiments to avoid the problems described in the previous chapter. Better measuring equipment may also be used in this case, such as a laser vibrometer, in order to measure the frequency and amplitude of oscillations accurately, as the Optron ® system did not perform well for pipes submerged in water.

Appendix A
A Note on Rigid Body Motion

One of the focuses of the research was the incidence of rigid body modes with flexible boundary conditions. It was undetermined how these would play a part in the derivation and modelling of the systems with a variable flexibility in their boundary conditions. In a limiting case, where the springs under consideration approach zero stiffness, should have the system attain pseudo-rigid body motion as its first mode of vibration. Thus, the possibility of introducing a new set of comparison functions similar to those of equation (2.27) was considered for the flexible models.

As the modes evolve with increasing flow velocity they merge and show elements of other modes. What is called ‘mode 2’ in an Argand diagram is, in reality, a mode composed of elements predominantly from the first, second and third mode, with the inclusion of other modes as well. However, if during the development of a mathematical model a mode is excluded, then the entire evolution of all the following modes lacks its contribution and therefore yields an erroneous dynamic behaviour of the model.

This problem became visible when the comparison between a standard pinned-free pipe and the new ‘pinned + c’-free model was made. The two did not match, and originally it was believed that it was the flexible model that was wrong. However, a careful look at the Argand diagram produced by the standard pinned-free pipe conveying fluid showed that the model was diverging by buckling for every single mode, with no flutter present.

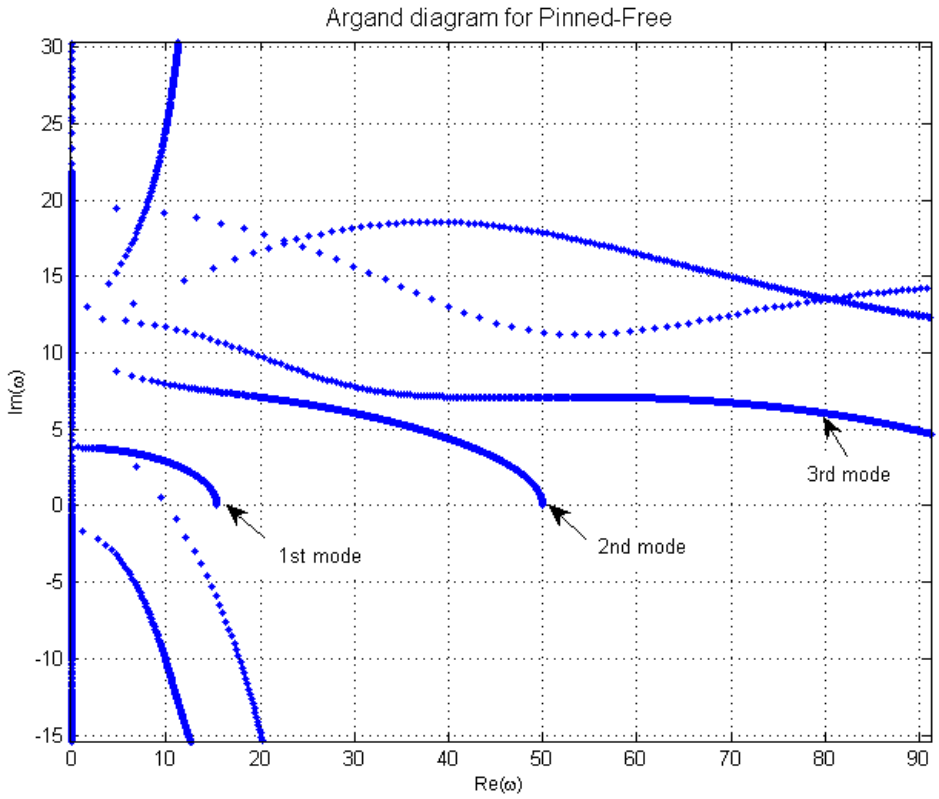

Figure 0.1 – Erroneous Argand diagram for a standard pinned-free pipe without accounting for rigid body motion ($\beta = 0.2$). There is only static divergence present.

This was a completely unexpected and unrealistic behaviour due to the non-conservative nature of the problem. It was then realized that the model was not taking into account rigid body motion. This had repercussions throughout the entire model due to the aforementioned reasons. The rigid body mode did not arise naturally from the derivation of the comparison functions (ϕ's) using the boundary conditions. To overcome this problem, they were derived manually, yielding equation (2.27) in subsection 2.2.2, which is restated here to aid the reader

$$\begin{aligned} \phi_1(\xi) &= \sqrt{3}\,\xi \ , \\ \phi_r(\xi) &= \sin(\lambda_r \xi) + \sigma_r \sinh(\lambda_r \xi) \ , \quad for\ r = 2,3,\dots,n \ . \end{aligned} \tag{A.1}$$

The corresponding rigid body eigenvalue of zero was found analytically by the Maple ® algorithm. To correct the Matlab ® program, the code was written to forcibly input the rigid

body mode into the mass ($[M]$), damping ($[C]$), and stiffness ($[K]$) matrices by displacing all currently existing parameters by one row and one column, in the following fashion:

$$[M] = \begin{bmatrix} f_1 & f_2 & f_3 \\ f_4 & f_5 & f_6 \\ f_7 & f_8 & f_9 \end{bmatrix} \rightarrow [M] = \begin{bmatrix} . & . & . & . \\ . & f_1 & f_2 & f_3 \\ . & f_4 & f_5 & f_6 \\ . & f_7 & f_8 & f_9 \end{bmatrix}, \qquad (A.2)$$

where the dots shown represent the shift of all entries by one row and one column. In the first row and first column all parameters were correctly multiplied by the new rigid body mode (ϕ_1) and its corresponding derivatives. This allowed the program to accurately account for the missing rigid-body mode and produced the correct Argand diagram for a pinned-free pipe.

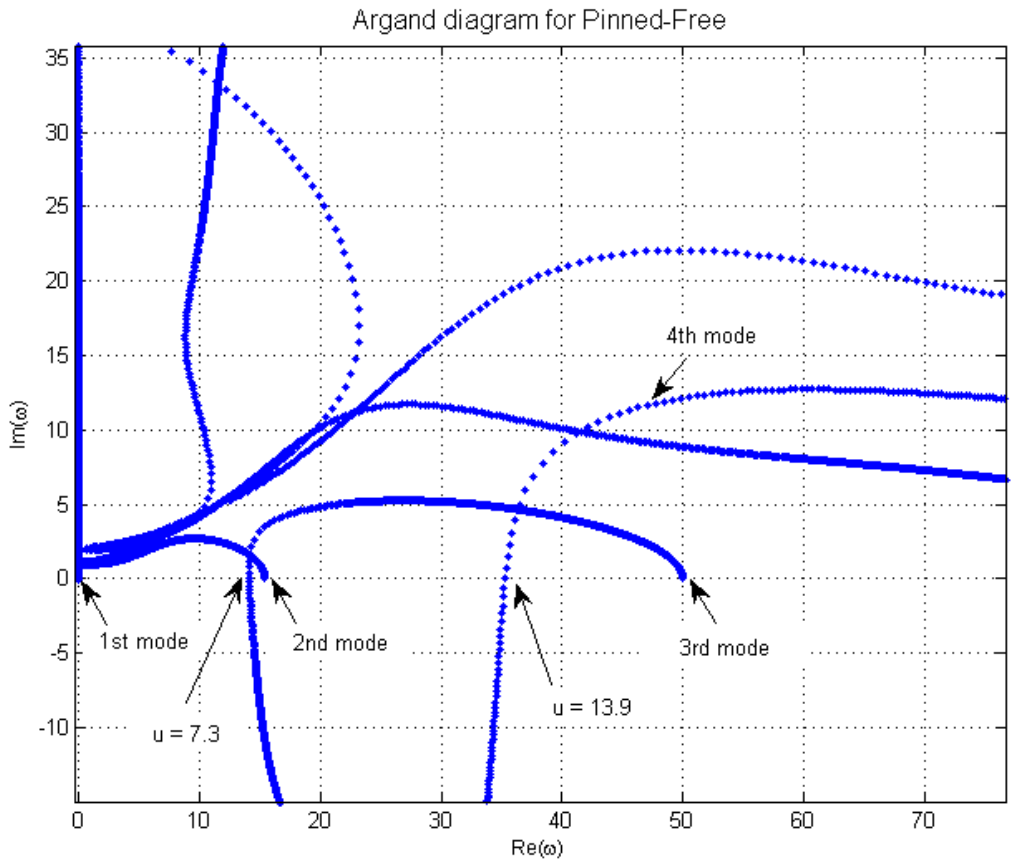

Figure 0.2 - Corrected Argand diagram for a standard pinned-free pipe, accounting for rigid body motion ($\beta = 0.2$). There is only static divergence present.

Appendix B
Pipe Casting Procedure

During the experiments several flexible elastomer pipes were used. These were cast tailored for this particular experiment by using *Dragon Skin* ® silicone from Smooth-On. A pipe-casting apparatus designed by Paidoussis (1998, Appendix D) was used for the process. All the equipment and materials used in the process are shown in Figure B.1. There were several steps required for the casting of the pipes, described by the following steps:

1. Start by opening the mould and carefully separating the top from the bottom (there are guider pins on the mould, making it easy to create a moment on the brittle plexiglas). Clean the mould, ensuring there are no remains from previous castings. Apply silicone release spray (Dow Corning ® 316) or another plastic releasing agent. Be sure to apply it to both sides of the mould as well as the central rod.
2. Next, open the top end of the plexiglas piston by unscrewing the top. Retract the piston to allow for a more in-depth cleaning. Again, clean the leftover silicone from previous castings carefully. Then apply silicone release spray (Dow Corning ® 316) or another suitable releasing agent.
3. Cover the holes at the end of one of the brass fittings to be used. This is to prevent the silicone plastic from spilling from the bottom once the mixture is poured into the mould.
4. Secure the center rod in place using the two corresponding brass fittings. Place the rod and the two fittings on the channel of the bottom part of the mould. Ensure that the innermost part of the brass fittings is sitting at the edge of the mould. The rod should not be touching the

mould. Place the mould cap in place following the guider pins. Then place the top and screw it in place tightly.

5. Prepare the silicone mix by using equal parts (a ratio of 1:1) of Dragon Skin Part A and Dragon Skin Part B. Mix in a contained that provides a wide surface area. Depending on the desired stiffness of the pipe, add solvent at discretion. The pipes used during the experiment had 1:1:0.25 and 1:1:0 ratios of all the products. Finally, add a few drops of colorant to dye the pipes white. Mix thoroughly by hand to avoid too many air inclusions.
6. Take the container and place it in the vacuum chamber. Let it be in the vacuum for around fifteen minutes, until all the air inclusions bubble out. Once ready, remove from the chamber slowly.
7. Have the plexiglas piston with the top unscrewed ready. Pour the silicon mixture very slowly into the piston, ensuring no air is trapped as it is poured. Once all the mix is inside, screw the top back in place tightly.
8. Rest the mould at an angle ready to receive the silicone from the piston (an angle of thirty degrees works fine). Use the connecting tube to tightly secure the uncovered brass fitting on the mould with the piston mouth. Pour the mixture into the mould very slowly.
9. Let the mould rest vertically by clamping it securely. Ensure that it is resting with the covered brass fitting facing down to avoid spilling the silicon mixture. Wait approximately five hours for the silicone to solidify.
10. After the five hours, carefully open up the mould by unscrewing the top. Remove the top and be careful not to damage the mould with the guider pins. Remove the pipe carefully with the center rod inside. Use the vacuum pump to introduce compressed air into the silicon pipe, thereby allowing for an easy release of the center rod.

11. Cut the jagged ends of the pipe to make it straight and smooth. Placing the pipe partially onto the rod will help keep it straight. Using a thin metal string (or a guitar string) works well for cutting the pipe. Make a loop around the end of the pipe and then constrict the pipe firmly and strongly to make a smooth cut. The pipe is now ready to be used.

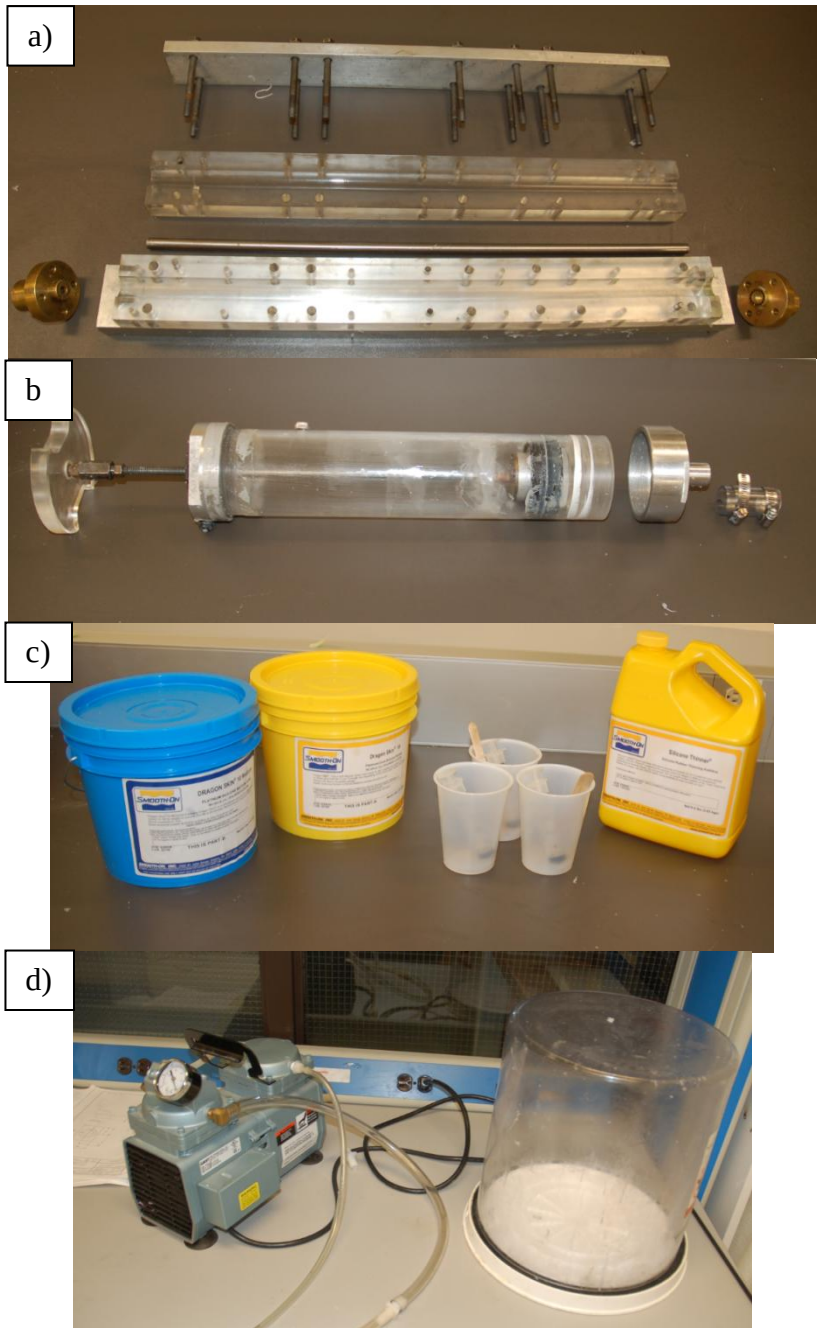

Figure 0.1 – Equipment for pipe casting: (a) Mould with center rod and brass fittings, (b) plexiglas piston with connecting tube, (c) Dragon Skin parts A & B and solvent, and (d) vacuum pump and chamber.

Appendix C
Obtaining the Properties of the Pipes

C.1 Obtaining the Flexural Rigidity

The purpose of this section is to explain how the flexural rigidity (EI) of the cast pipes was obtained. The natural frequencies of each pipe for the first three modes were found by exciting the pipes with an arbitrary forcing frequency. This was achieved by using a mechanical exciter and having the pipe hanging vertically from a clamped support (see Figure C.3). The frequencies were then measured using the Optron ® system as the pipe oscillations decayed. The output was given by a LabVIEW ® interface which tabulated all the data. This information was then processed in Matlab ® by the use of a power spectral density (PSD) plot to obtain the highest peaks from the frequency obtained. These correspond to the natural frequencies of the pipe. The process was repeated enough times to accurately determine the first three natural frequencies of the system. The following relationship was the used:

$$\frac{\gamma}{\left[Re(\omega_j)\right]^2} = \frac{g}{\left[Re(\Omega_j)\right]^2 L}, \qquad (C.1)$$

where g is the free-fall acceleration constant and $\gamma = mgL^3/EI$ its nondimensional counterpart, $\Omega_j = 2\pi f_j$ is the j[th] frequency of vibration in radians per second and $\omega_j = \left(\frac{M+m}{EI}\right)^{\frac{1}{2}} \Omega_j L^2$ its nondimensional counterpart, and L the total length of the pipe. One can easily obtain the value of the right-hand side of equation (C.1) and then use this value to interpolate (or extrapolate) from the tables given by Paidoussis & des Trois Maisons (1971). In this particular case the plot in Figure C.1 was produced by using a line of best-fit on the tabulated points.

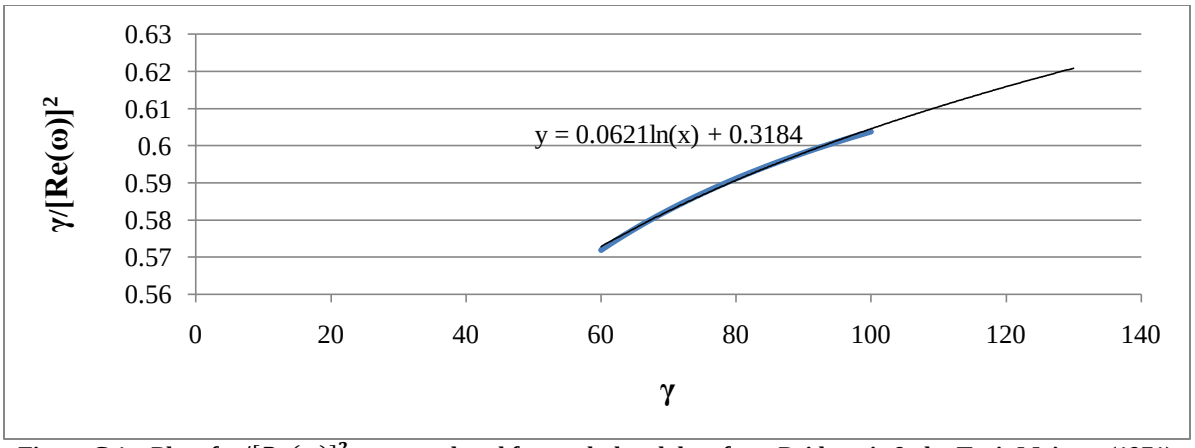

Figure C.1 – Plot of $\gamma/[Re(\omega)]^2$ vs. γ produced from tabulated data from Paidoussis & des Trois Maisons (1971)

From the equation of the best-fit curve the value of γ may be obtained. In turn, γ can be used to obtained the flexural rigidity from the following relationship

$$\gamma = \frac{mgL^3}{EI}, \qquad (C.2)$$

where m is the mass per unit length of the pipe. To have a good approximation of the real flexural rigidity, it is advised to do the process outlined for each of the natural frequencies recorded and then obtaining an average.

C.2 Obtaining the Kelvin-Voigt Type Dissipation Constant

To obtain the Kelvin-Voigt type dissipation constant it is required to first obtain the logarithmic decrement for the first three modes. This can be done by exciting the pipe using the mechanical exciter and setting the forcing frequency equal to each of the natural frequencies. Then allow the pipe oscillations to decay and record this with the Optron ® system. Use a filter (LabVIEW ® has some built-in filters) to obtain the logarithmic decrement corresponding to each frequency. Then process the data in Matlab ® and obtain the logarithmic decrements. Use Figures 1 and 2 from Paidoussis & des Trois Maisons (1971) to obtain the relationship of the logarithmic decrements with the viscoelastic dissipation. For this thesis, the hysteretic model of

damping was neglected and all the dissipative properties were lumped in the Kelvin-Voigt type dissipation. Therefore, assume the following:

$$\delta_n^* = \frac{\delta_n}{\mu + \alpha\, Re(\omega_n)} \cong \frac{\delta_n}{\alpha\, Re(\omega_n)} \qquad (C.3)$$

The plot in Figure C.2 was used to extrapolate data from Figures 1 and 2. The result is the following

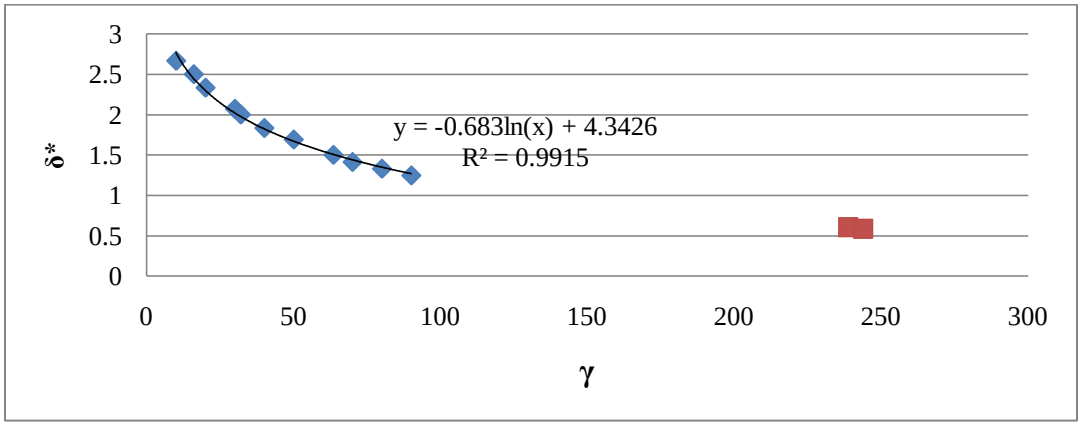

Figure C.2 – Logarithmic decrement plot obtained from information from Paidoussis & des Trois Maisons (1971)

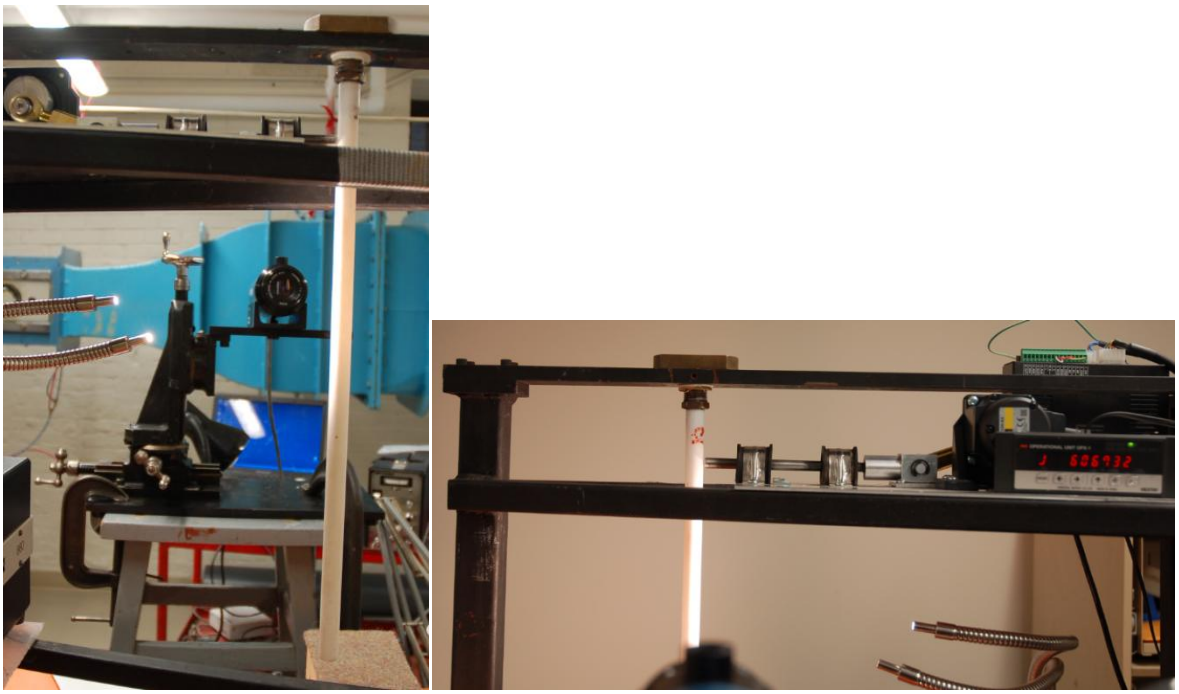

Figure C.3 – Exciter with pipe in place and Optron system

Appendix D
Matlab ® Code for Mathematical Models

All the mathematical models used throughout the research were programmed and executed in Matlab ® (v. R2009b). It is important to point out that a Maple ® (v. 15) analytical toolbox was installed and executed from Matlab ® when producing the models.

The development of the code underwent several changes and improvements throughout the time invested in the research. The first major improvement came for the root-finding algorithm used to find the eigenvalues from the characteristic equation. Instead of using a numerical method from Matlab ®, the Maple ® toolbox was installed and used to have an analytical solution to the problem. This increased accuracy and sped up computing time. Output was also much easier to handle. The next step came when the Galerkin method was developed. The code was written in such a way that the comparison functions were evaluated for every cell in each of the three matrices (mass matrix, damping matrix, stiffness matrix). The first attempt used a Gaussian quadrature (Kiusalaas, 2005) to approximate the integrals of the comparison functions. Accuracy was verified with analytical results in Maple ®. Analytical integration was not used due to the computing power required. Still, the numerical method of using a quadrature still had a toll on computing speed. Thus, the method was later replaced by a Simpson's rule approach (Kiusalaas, 2005).

The codes for each pipe configuration discussed in the thesis are presented in the next few pages, with all the user-built functions shown at the end as well.

D.1 Pinned-Free Pipe Conveying Fluid Model - Matlab ® Code

```
%%  Pinned-Free pipe COMPLETE
%% Beam Eigenfunctions and Eigenvalues
clear all
clc
close all
format long
tic
syms lambda;
maple('Digits:=15');
maple('with(Student[Calculus1])');
maple('with(ArrayTools)');
maple('f := tan(lambda)-tanh(lambda)');
b = maple('Roots(f = 0, lambda = -1 .. 30, numeric)'); % lambda = lambda * L
b = transpose(double(b)); % Beam Eigenvalues
clear lambda
%% Define Parameters of the system
c = 0; % Rotational spring constant, *not applicable to this problem*
k = 0; % Translational spring constant, *not applicable for this problem*
g = 0; % Non-dim gravity parameter (gamma)
a = 0; % Kelvin-Voigt non-dim E* parameter (alpha)
T = 0; % Non-dim tension parameter - ZERO always for cantilevered
P = 0; % Non-dim pressure parameter (Pi) - ZERO always for cantilevered
poisson = 0; % Poisson's ratio of the material (nu)
delta = 0; % If delta = 0, no constraint in the axial motion, if delta = 1, there
is
sigma = 0; % Non-dim dissipation to the surrounding fluid
beta = 0.2; % Non-dim mass ratio
KK = 0; % Non-dim distributed stiffness per unit length
Udot = 0; % Acceleration of fluid-flow velocity (should be 0)
BC = 'pinned'; % Define type of BC's from: free, pinned, clamped, pinned+c,
free+c+k
%% Galerkin Method for various fluid flow velocities
counter = 0;
[modes,Null] = size(b); % Number of modes used in the approximation= number of
eigenvalues found in the specifried interval
u_max = 10;
step = 0.02; % Step increase for flow velocity, u
initial = 0; % Initial velocity

ForMovie = zeros((1+(u_max-initial)/step)*2*modes,1);
ForU_cr = zeros((1+(u_max-initial)/step)*2*modes,2);
Im_freq = zeros(1 + u_max/step, 2*modes);
Re_freq = zeros(1 + u_max/step, 2*modes);
ForPlot = zeros(1+ u_max/step, 4*modes);
im = sqrt(-1);

for u = initial:step:u_max
    counter = counter + 1
    K = zeros(modes,modes);
    M = zeros(modes,modes);
    C = zeros(modes,modes);
```

Continued

```
    % Mass matrix + rigid body modes
    for j = 2:modes
        for i = 2:modes
            Li = b(i);
            if i==j
                M(j,i) = phi_phi(BC,Li,c,k); else
                M(j,i) = 0;
            end
        end
    end
    M(1,1) = 1;

    % Dissipation matrix + rigid body modes
    for j = 2:modes
        lambda = b(j);
        rigid_phi1_Rphi = @(x) (sqrt(3))*(sin(lambda * x) + 0.1e1 / sinh(lambda) *
sin(lambda) * sinh(lambda * x));
        C(j,1) = 2*u*beta^0.5*quad(rigid_phi1_Rphi,0,1);
        clear lambda
        for i = 2:modes
            Li = b(i);
            Lj = b(j);
            if i==j
                C(j,i)=2*u*beta^0.5*phi1_phi(BC,Li,Lj,c,k) +
sigma*phi_phi(BC,Li,c,k) + a*b(i)^4*phi_phi(BC,Li,c,k); else
                C(j,i)=2*u*beta^0.5*phi1_phi(BC,Li,Lj,c,k);
            end
        end
    end
    C(1,1) = 2*u*beta^0.5*1.5 + sigma;
    for i=2:modes
        L = b(i);
        rigid_phi12_phi =@(x) (sqrt(3)*x).*(cos(L * x) * L + 0.1e1 / sinh(L) *
sin(L) * cosh(L * x) * L);
        C(1,i) = 2*u*beta^0.5*quad(rigid_phi12_phi,0,1);
        clear L
    end

    % Stiffness matrix + rigid body modes
    for j = 2:modes
        lambda = b(j);
        rigid_phi1_Rphi = @(x) (sqrt(3))*(sin(lambda * x) + 0.1e1 / sinh(lambda) *
sin(lambda) * sinh(lambda * x));
        K(j,1) = g*quad(rigid_phi1_Rphi,0,1);
        clear lambda
        for i = 2:modes
            Li = b(i);
            Lj = b(j);
```

Continued

```
            if i==j
               K(j,i) = b(i)^4*phi_phi(BC,Li,c,k) + u^2*phi2_phi(BC,Li,Lj,c,k) +
g*phi1_phi(BC,Li,Lj,c,k) + g*phi2_phi_x(BC,Li,Lj,c,k) + KK*phi_phi(BC,Li,c,k) +
P*(1 - 2*poisson*delta)*phi2_phi(BC,Li,Lj,c,k) - T*phi2_phi(BC,Li,Lj,c,k); else
               K(j,i) = u^2*phi2_phi(BC,Li,Lj,c,k) + g*phi1_phi(BC,Li,Lj,c,k) +
g*phi2_phi_x(BC,Li,Lj,c,k) + P*(1 - 2*poisson*delta)*phi2_phi(BC,Li,Lj,c,k) -
T*phi2_phi(BC,Li,Lj,c,k);
            end
        end
    end

    K(1,1) = 0;
    clear lambda
    for i=2:modes
        L = b(i);
        phi21_phi =@(x) (sqrt(3)*x).*(-sin(L * x) * L ^ 2 + 0.1e1 / sinh(L) *
sin(L) * sinh(L * x) * L ^ 2);
        rigid_phi12_phi =@(x) (sqrt(3)*x).*(cos(L * x) * L + 0.1e1 / sinh(L) *
sin(L) * cosh(L * x) * L);
        K(1,i) = (u^2 + g)*quad(phi21_phi,0,1) + g*quad(rigid_phi12_phi,0,1);
        clear L
    end

    % Set up the inverse dynamical matrix
    O = zeros(modes,modes);
    B = [O M; M C];
    E = [-M O; O K];
    Y = B\E;

    [mode_shape,omega_squared]=eig(Y,'nobalance'); %extracting the eigenvalues
    omega = sqrt(omega_squared);

    nat_freq = 1:(2*modes);
    for i=1:(2*modes)
        nat_freq(i) = omega_squared(i,i);
    end

    nat_freq = transpose(nat_freq);
    u_vector = u*ones(2*modes, 1);
    ForMovie((counter-1)*2*modes+1:(counter*2*modes)) = (im*nat_freq);
    ForU_cr([(counter-1)*2*modes+1:(counter*2*modes) (counter-
1)*2*modes+1:(counter*2*modes)]) = ([(im*nat_freq) u_vector]);

    for i=1:(2*modes);
        Im_freq(counter,i) = real(nat_freq(i));
        Re_freq(counter,i) = abs(imag(nat_freq(i)));
    end
end
```

Continued

```
%% Create a matrix with Re&Im next to each other
for i = 1:(2*modes)
    ForPlot(:,i*2-1) = Re_freq(:,i);
    ForPlot(:,i*2) = Im_freq(:,i);
end

%% Plot Results in Argand Diagram
for i = 1:(modes*2)
    plot(ForPlot(:,2*i-1),ForPlot(:,2*i),'.','MarkerSize',6)
    title('Argand diagram for Pinned-Free', 'FontSize',12);
    xlabel('Re(\omega)','FontSize',9);
    ylabel('Im(\omega)','FontSize',9);
    hold on
    grid on
end

%% Plot Results for Im(w) vs u
figure;
ForU_cr = sortrows(ForU_cr);
plot(ForU_cr(:,1),imag(ForMovie),'.','MarkerSize',6)
title('Im(\omega) vs u for Pinned-Free', 'FontSize',12);
xlabel('u','FontSize',9);
ylabel('Im(\omega)','FontSize',9);
hold on
grid on
U_crVector = [ForU_cr(:,1) imag(ForMovie)];
counter2 = 0;
for i = 1:size(U_crVector)
    if abs(U_crVector(i,2)) < 0.09
        counter2 = counter2 + 1;
        U_crPoints(counter2,:) = U_crVector(i,:);
    end
end
U_crPoints = removeRepeatedElements(U_crPoints);

%% Produe Argand plot Movie
ArgandMovie2('trialmovie.avi',modes*2,ForMovie);

toc
```

D.2 General Pipe Conveying Fluid Model - Matlab ® Code

The following is the general code used for most of the problems (with explicit rigid body modes). Several lines of command are not active (%_) as they correspond to the different configurations used. These are identified in the inline comments as 'clamped' (classic cantilevered pipe), 'free' (for a free-free pipe), 'pinned + c' (pinned-free pipe with rotational spring at origin), and 'free + c + k' (free-free pipe with rotational and translational springs at origin). Further explanation can be found in the inline comments.

```
%% General pipe with k & c COMPLETE
%% Beam Eigenfunctions and Eigenvalues
clear all
clc
format long
close all
tic
syms lambda;
maple('Digits:=15');
maple('with(Student[Calculus1])');
maple('with(ArrayTools)');
maple('c:= 10^(1.25)'); % Select value for c
maple('k:= 100'); % Select Value for k

% Clamped
% maple('f := cosh(lambda) * lambda ^ 2 + cos(lambda) * lambda ^ 2 - (sinh(lambda)
- sin(lambda)) / (cosh(lambda) + cos(lambda)) * (sinh(lambda) * lambda ^ 2 +
sin(lambda) * lambda ^ 2)');

% Free
% maple('f := cos(lambda)*cosh(lambda)-1');

% Pinned+c
% maple('f := -c * (sin(lambda) + sinh(lambda)) / (0.2e1 * lambda * sinh(lambda) +
c * cos(lambda) + c * cosh(lambda)) * sin(lambda) * lambda ^ 3 + c * (sin(lambda) +
sinh(lambda)) / (0.2e1 * lambda * sinh(lambda) + c * cos(lambda) + c *
cosh(lambda)) * sinh(lambda) * lambda ^ 3 - cos(lambda) * lambda ^ 3 - 0.1e1 /
(0.2e1 * lambda * sinh(lambda) + c * cos(lambda) + c * cosh(lambda)) * (-0.2e1 *
sin(lambda) * lambda + c * cos(lambda) + c * cosh(lambda)) * cosh(lambda) * lambda
^ 3');
```

Continued

```
% Free+c+k
maple('f := (-lambda ^ 4 + 0.2e1 * c * (-cosh(lambda) * (-lambda ^ 4 + c * k) -
cos(lambda) * lambda ^ 4 - cos(lambda) * c * k + 0.2e1 * sin(lambda) * k * lambda)
/ (-0.2e1 * cos(lambda) * c * lambda ^ 3 + sin(lambda) * lambda ^ 4 + sin(lambda) *
c * k - sinh(lambda) * lambda ^ 4 + sinh(lambda) * c * k) * lambda ^ 3 - c * k) /
(-lambda ^ 4 + c * k) * sin(lambda) * lambda ^ 3 + sinh(lambda) * lambda ^ 3 + (-(-
cosh(lambda) * (-lambda ^ 4 + c * k) - cos(lambda) * lambda ^ 4 - cos(lambda) * c *
k + 0.2e1 * sin(lambda) * k * lambda) / (-0.2e1 * cos(lambda) * c * lambda ^ 3 +
sin(lambda) * lambda ^ 4 + sin(lambda) * c * k - sinh(lambda) * lambda ^ 4 +
sinh(lambda) * c * k) * lambda ^ 3 + k * ((-lambda ^ 4 + 0.2e1 * c * (-cosh(lambda)
* (-lambda ^ 4 + c * k) - cos(lambda) * lambda ^ 4 - cos(lambda) * c * k + 0.2e1 *
sin(lambda) * k * lambda) / (-0.2e1 * cos(lambda) * c * lambda ^ 3 + sin(lambda) *
lambda ^ 4 + sin(lambda) * c * k - sinh(lambda) * lambda ^ 4 + sinh(lambda) * c *
k) * lambda ^ 3 - c * k) / (-lambda ^ 4 + c * k) + 0.1e1)) * cos(lambda) + (-
cosh(lambda) * (-lambda ^ 4 + c * k) - cos(lambda) * lambda ^ 4 - cos(lambda) * c *
k + 0.2e1 * sin(lambda) * k * lambda) / (-0.2e1 * cos(lambda) * c * lambda ^ 3 +
sin(lambda) * lambda ^ 4 + sin(lambda) * c * k - sinh(lambda) * lambda ^ 4 +
sinh(lambda) * c * k) * cosh(lambda) * lambda ^ 3');
b = maple('Roots(f = 0, lambda = 0 .. 30, numeric)'); % lambda = lambda * L
b = transpose(double(b)); % Beam Eigenvalues
clear lambda
%% Define Parameters of the system
c = double(maple('c'));
k = double(maple('k'));
kk = 0; % Translational spring constant, *not applicable for this problem*
g = 0; % Non-dim gravity parameter (gamma)
a = 0; % Kelvin-Voigt non-dim E* parameter (alpha)
T = 0; % Non-dim tension parameter - ZERO always for cantilevered
P = 0; % Non-dim pressure parameter (Pi) - ZERO always for cantilevered
poisson = 0; % Poisson's ratio of the material (nu)
delta = 0; % If delta = 0, no constraint in the axial motion, if delta = 1, there
is
sigma = 0; % Non-dim dissipation to the surrounding fluid
beta = 0.2; % Non-dim mass ratio
KK = 0; % Non-dim distributed stiffness per unit length
Udot = 0; % Acceleration of fluid-flow velocity (should be 0)
BC = 'free+c+k'; % Define type of BC's from: free, pinned, clamped, pinned+c,
free+c+k
%% Galerkin Method for various fluid flow velocities
counter = 0;
[modes,Null] = size(b); % Number of modes used in the approximation= number of
eigenvalues found in the specified interval
u_max = 10; % Maximum fluid-flow velocity
step = 0.02; % Step increase for flow velocity, u

ForMovie = zeros((1+u_max/step)*2*modes,1);
ForU_cr = zeros((1+u_max/step)*2*modes,2);
Im_freq = zeros(1 + u_max/step, 2*modes);
Re_freq = zeros(1 + u_max/step, 2*modes);
ForPlot = zeros(1+ u_max/step, 4*modes);
im = sqrt(-1);
```

Continued

```
for u = 0:step:u_max
    counter = counter + 1
    K = zeros(modes,modes);
    M = zeros(modes,modes);
    C = zeros(modes,modes);

    % Mass matrix
    for j = 1:modes
        for i = 1:modes
            Li = b(i);
            if i==j
                M(j,i) = phi_phi(BC,Li,c,k); else
                M(j,i) = 0;
            end
        end
    end

    % Dissipation matrix
    for j = 1:modes
        for i = 1:modes
            Li = b(i);
            Lj = b(j);
            if i==j
                C(j,i)=2*u*beta^0.5*phi1_phi(BC,Li,Lj,c,k) +
sigma*phi_phi(BC,Li,c,k) + a*b(i)^4*phi_phi(BC,Li,c,k); else
                C(j,i)=2*u*beta^0.5*phi1_phi(BC,Li,Lj,c,k);
            end
        end
    end

    % Stiffness matrix
    for j = 1:modes
        for i = 1:modes
            Li = b(i);
            Lj = b(j);
            if i==j
                K(j,i) = b(i)^4*phi_phi(BC,Li,c,k) + u^2*phi2_phi(BC,Li,Lj,c,k) +
g*phi1_phi(BC,Li,Lj,c,k) + g*phi2_phi_x(BC,Li,Lj,c,k) + KK*phi_phi(BC,Li,c,k) +
P*(1 - 2*poisson*delta)*phi2_phi(BC,Li,Lj,c,k) - T*phi2_phi(BC,Li,Lj,c,k); else
                K(j,i) = u^2*phi2_phi(BC,Li,Lj,c,k) + g*phi1_phi(BC,Li,Lj,c,k) +
g*phi2_phi_x(BC,Li,Lj,c,k) + P*(1 - 2*poisson*delta)*phi2_phi(BC,Li,Lj,c,k) -
T*phi2_phi(BC,Li,Lj,c,k);
            end
        end
    end

    % Set up the inverse dynamical matrix
    O = zeros(modes,modes);
    B = [O M; M C];
    E = [-M O; O K];
    Y = B\E;
```

Continued

```
    [mode_shape,omega_squared]=eig(Y,'nobalance'); %extracting the eigenvalues
    omega = sqrt(omega_squared);

    nat_freq = 1:(2*modes);
    for i=1:(2*modes)
        nat_freq(i) = omega_squared(i,i);
    end

    nat_freq = transpose(nat_freq);
    u_vector = u*ones(2*modes, 1);
    ForMovie((counter-1)*2*modes+1:(counter*2*modes)) = (im*nat_freq);
    ForU_cr([(counter-1)*2*modes+1:(counter*2*modes) (counter-
1)*2*modes+1:(counter*2*modes)]) = ([(im*nat_freq) u_vector]);

    for i=1:(2*modes);
        Im_freq(counter,i) = real(nat_freq(i));
        Re_freq(counter,i) = abs(imag(nat_freq(i)));
    end
end
%% Create a matrix with Re&Im next to each other
for i = 1:(2*modes)
    ForPlot(:,i*2-1) = Re_freq(:,i);
    ForPlot(:,i*2) = Im_freq(:,i);
end

%% Plot Results in Argand Diagram
for i = 1:(modes*2)
    plot(ForPlot(:,2*i-1),ForPlot(:,2*i),'.','MarkerSize',6)
    title('Argand diagram for Free-Free with c = 10^1^2 and k = 10^1^2',
'FontSize',12);
    xlabel('Re(\omega)','FontSize',9);
    ylabel('Im(\omega)','FontSize',9);
    hold on
    grid on
end

%% Plot Results for Im(w) vs u
figure;
ForU_cr = sortrows(ForU_cr);
plot(ForU_cr(:,1),imag(ForMovie),'.','MarkerSize',6)
title('Im(\omega) vs u for Free-Free with c = 10^1^2 and k = 10^1^2',
'FontSize',12);
xlabel('u','FontSize',9);
ylabel('Im(\omega)','FontSize',9);
hold on
grid on
U_crVector = [ForU_cr(:,1) imag(ForMovie)];
```

Continued

```
counter2 = 0;
for i = 1:size(U_crVector)
    if abs(U_crVector(i,2)) < 0.09
        counter2 = counter2 + 1;
        U_crPoints(counter2,:) = U_crVector(i,:);
    end
end
U_crPoints = removeRepeatedElements(U_crPoints);

%% Produe Argand plot Movie
ArgandMovie2('trialmovie.avi',modes*2,ForMovie);

toc
```

D.3 User-built Functions for Matlab ®

There are several functions used in the programs given before. The code for these will be given in the following pages.

D.3.1 Function phi_phi

```
function y = phi_phi(BC,Li,c,k)

N = 199;
h = 1/(N-1);
x = (0:h:1);
w = ones(1,N);
w(2:2:N-1) = 4;
w(3:2:N-2) = 2;
w = w*h/3;

if strcmp(BC,'clamped') == 1
    y = 1;
elseif strcmp(BC,'pinned') == 1
    y = 0.5;
elseif strcmp(BC,'pinned+c') == 1
    y = sum(w.*(-c * (sin(Li) + sinh(Li)) / (0.2e1 * Li * sinh(Li) + c * cos(Li) +
c * cosh(Li)) * cos(Li * x) + c * (sin(Li) + sinh(Li)) / (0.2e1 * Li * sinh(Li) + c
* cos(Li) + c * cosh(Li)) * cosh(Li * x) + sin(Li * x) - 0.1e1 / (0.2e1 * Li *
sinh(Li) + c * cos(Li) + c * cosh(Li)) * (-0.2e1 * sin(Li) * Li + c * cos(Li) + c *
cosh(Li)) * sinh(Li * x)).*(-c * (sin(Li) + sinh(Li)) / (0.2e1 * Li * sinh(Li) + c
* cos(Li) + c * cosh(Li)) * cos(Li * x) + c * (sin(Li) + sinh(Li)) / (0.2e1 * Li *
sinh(Li) + c * cos(Li) + c * cosh(Li)) * cosh(Li * x) + sin(Li * x) - 0.1e1 /
(0.2e1 * Li * sinh(Li) + c * cos(Li) + c * cosh(Li)) * (-0.2e1 * sin(Li) * Li + c *
cos(Li) + c * cosh(Li)) * sinh(Li * x)));
```

Continued

```
elseif strcmp(BC,'free+c+k') == 1
    y = sum(w.*(-(-Li ^ 4 * sin(Li) + c * k * sin(Li) + Li ^ 4 * sinh(Li) + c * k *
sinh(Li) + 0.2e1 * Li ^ 3 * cosh(Li) * c) / (-cos(Li) * Li ^ 4 + cos(Li) * c * k +
cosh(Li) * Li ^ 4 + cosh(Li) * c * k + 0.2e1 * Li * sinh(Li) * k) * cos(Li * x) -
(0.2e1 * Li ^ 3 * cos(Li) * c - Li ^ 4 * sin(Li) - c * k * sin(Li) + Li ^ 4 *
sinh(Li) - c * k * sinh(Li)) / (-cos(Li) * Li ^ 4 + cos(Li) * c * k + cosh(Li) * Li
^ 4 + cosh(Li) * c * k + 0.2e1 * Li * sinh(Li) * k) * cosh(Li * x) + sin(Li * x) -
0.1e1 / (-cos(Li) * Li ^ 4 + cos(Li) * c * k + cosh(Li) * Li ^ 4 + cosh(Li) * c * k
+ 0.2e1 * Li * sinh(Li) * k) * (cos(Li) * Li ^ 4 + cos(Li) * c * k - cosh(Li) * Li
^ 4 + cosh(Li) * c * k - 0.2e1 * Li * sin(Li) * k) * sinh(Li * x)).*(-(-Li ^ 4 *
sin(Li) + c * k * sin(Li) + Li ^ 4 * sinh(Li) + c * k * sinh(Li) + 0.2e1 * Li ^ 3 *
cosh(Li) * c) / (-cos(Li) * Li ^ 4 + cos(Li) * c * k + cosh(Li) * Li ^ 4 + cosh(Li)
* c * k + 0.2e1 * Li * sinh(Li) * k) * cos(Li * x) - (0.2e1 * Li ^ 3 * cos(Li) * c
- Li ^ 4 * sin(Li) - c * k * sin(Li) + Li ^ 4 * sinh(Li) - c * k * sinh(Li)) / (-
cos(Li) * Li ^ 4 + cos(Li) * c * k + cosh(Li) * Li ^ 4 + cosh(Li) * c * k + 0.2e1 *
Li * sinh(Li) * k) * cosh(Li * x) + sin(Li * x) - 0.1e1 / (-cos(Li) * Li ^ 4 +
cos(Li) * c * k + cosh(Li) * Li ^ 4 + cosh(Li) * c * k + 0.2e1 * Li * sinh(Li) * k)
* (cos(Li) * Li ^ 4 + cos(Li) * c * k - cosh(Li) * Li ^ 4 + cosh(Li) * c * k -
0.2e1 * Li * sin(Li) * k) * sinh(Li * x)));
elseif strcmp(BC,'free') == 1
    y = 1;
elseif strcmp(BC,'pinned-pinned') == 1
    y = 1;
end
```

D.3.2 Function phi1_phi

```
function y = phi1_phi(BC,Li,Lj,c,k)

N = 199;
h = 1/(N-1);
x = (0:h:1);
w = ones(1,N);
w(2:2:N-1) = 4;
w(3:2:N-2) = 2;
w = w*h/3;

if strcmp(BC,'clamped') == 1
    y = sum(w.*(sinh(Li * x) * Li + sin(Li * x) * Li - (sinh(Li) - sin(Li)) /
(cosh(Li) + cos(Li)) * (cosh(Li * x) * Li - cos(Li * x) * Li)).*(cosh(Lj * x) -
cos(Lj * x) - (sinh(Lj) - sin(Lj)) / (cosh(Lj) + cos(Lj)) * (sinh(Lj * x) - sin(Lj
* x))));
elseif strcmp(BC,'pinned') == 1
    y = sum(w.*(cos(Li * x) * Li + 0.1e1 / sinh(Li) * sin(Li) * cosh(Li * x) *
Li).*(sin(Lj * x) + 0.1e1 / sinh(Lj) * sin(Lj) * sinh(Lj * x)));
```

Continued

```
elseif strcmp(BC,'pinned+c') == 1
    y = sum(w.*(c * (sin(Li) + sinh(Li)) / (0.2e1 * Li * sinh(Li) + c * cos(Li) + c
* cosh(Li)) * sin(Li * x) * Li + c * (sin(Li) + sinh(Li)) / (0.2e1 * Li * sinh(Li)
+ c * cos(Li) + c * cosh(Li)) * sinh(Li * x) * Li + cos(Li * x) * Li - 0.1e1 /
(0.2e1 * Li * sinh(Li) + c * cos(Li) + c * cosh(Li)) * (-0.2e1 * sin(Li) * Li + c *
cos(Li) + c * cosh(Li)) * cosh(Li * x) * Li).*(-c * (sin(Lj) + sinh(Lj)) / (0.2e1 *
Lj * sinh(Lj) + c * cos(Lj) + c * cosh(Lj)) * cos(Lj * x) + c * (sin(Lj) +
sinh(Lj)) / (0.2e1 * Lj * sinh(Lj) + c * cos(Lj) + c * cosh(Lj)) * cosh(Lj * x) +
sin(Lj * x) - 0.1e1 / (0.2e1 * Lj * sinh(Lj) + c * cos(Lj) + c * cosh(Lj)) * (-
0.2e1 * sin(Lj) * Lj + c * cos(Lj) + c * cosh(Lj)) * sinh(Lj * x)));
elseif strcmp(BC,'free+c+k') == 1
    y = sum(w.*((-Li ^ 4 * sin(Li) + c * k * sin(Li) + Li ^ 4 * sinh(Li) + c * k *
sinh(Li) + 0.2e1 * Li ^ 3 * cosh(Li) * c) / (-cos(Li) * Li ^ 4 + cos(Li) * c * k +
cosh(Li) * Li ^ 4 + cosh(Li) * c * k + 0.2e1 * Li * sinh(Li) * k) * sin(Li * x) *
Li - (0.2e1 * Li ^ 3 * cos(Li) * c - Li ^ 4 * sin(Li) - c * k * sin(Li) + Li ^ 4 *
sinh(Li) - c * k * sinh(Li)) / (-cos(Li) * Li ^ 4 + cos(Li) * c * k + cosh(Li) * Li
^ 4 + cosh(Li) * c * k + 0.2e1 * Li * sinh(Li) * k) * sinh(Li * x) * Li + cos(Li *
x) * Li - 0.1e1 / (-cos(Li) * Li ^ 4 + cos(Li) * c * k + cosh(Li) * Li ^ 4 +
cosh(Li) * c * k + 0.2e1 * Li * sinh(Li) * k) * (cos(Li) * Li ^ 4 + cos(Li) * c * k
- cosh(Li) * Li ^ 4 + cosh(Li) * c * k - 0.2e1 * Li * sin(Li) * k) * cosh(Li * x) *
Li).*(-(-Lj ^ 4 * sin(Lj) + c * k * sin(Lj) + Lj ^ 4 * sinh(Lj) + c * k * sinh(Lj)
+ 0.2e1 * Lj ^ 3 * cosh(Lj) * c) / (-cos(Lj) * Lj ^ 4 + cos(Lj) * c * k + cosh(Lj)
* Lj ^ 4 + cosh(Lj) * c * k + 0.2e1 * Lj * sinh(Lj) * k) * cos(Lj * x) - (0.2e1 *
Lj ^ 3 * cos(Lj) * c - Lj ^ 4 * sin(Lj) - c * k * sin(Lj) + Lj ^ 4 * sinh(Lj) - c *
k * sinh(Lj)) / (-cos(Lj) * Lj ^ 4 + cos(Lj) * c * k + cosh(Lj) * Lj ^ 4 + cosh(Lj)
* c * k + 0.2e1 * Lj * sinh(Lj) * k) * cosh(Lj * x) + sin(Lj * x) - 0.1e1 / (-
cos(Lj) * Lj ^ 4 + cos(Lj) * c * k + cosh(Lj) * Lj ^ 4 + cosh(Lj) * c * k + 0.2e1 *
Lj * sinh(Lj) * k) * (cos(Lj) * Lj ^ 4 + cos(Lj) * c * k - cosh(Lj) * Lj ^ 4 +
cosh(Lj) * c * k - 0.2e1 * Lj * sin(Lj) * k) * sinh(Lj * x)));
elseif strcmp(BC,'free') == 1
    y = sum(w.*(sinh(Li * x) * Li - sin(Li * x) * Li - (cosh(Li) - cos(Li)) /
(sinh(Li) - sin(Li)) * (cosh(Li * x) * Li + cos(Li * x) * Li)).*(cosh(Lj * x) +
cos(Lj * x) - (cosh(Lj) - cos(Lj)) / (sinh(Lj) - sin(Lj)) * (sinh(Lj * x) + sin(Lj
* x))));
elseif strcmp(BC,'pinned-pinned') == 1
    y = sum(w.*(sqrt(0.2e1) * cos(Li * x) * Li).*(sqrt(0.2e1) * sin(Lj * x)));
end
```

D.3.3 Function phi2_phi

```
function y = phi2_phi(BC,Li,Lj,c,k)

N = 199;
h = 1/(N-1);
x = (0:h:1);
w = ones(1,N);
w(2:2:N-1) = 4;
w(3:2:N-2) = 2;
w = w*h/3;

if strcmp(BC,'clamped') == 1
    y = sum(w.*(cosh(Li * x) * Li ^ 2 + cos(Li * x) * Li ^ 2 - (sinh(Li) - sin(Li))
/ (cosh(Li) + cos(Li)) * (sinh(Li * x) * Li ^ 2 + sin(Li * x) * Li ^ 2)).*(cosh(Lj
* x) - cos(Lj * x) - (sinh(Lj) - sin(Lj)) / (cosh(Lj) + cos(Lj)) * (sinh(Lj * x) -
sin(Lj * x))));
elseif strcmp(BC,'pinned') == 1
    y = sum(w.*(-sin(Li * x) * Li ^ 2 + 0.1e1 / sinh(Li) * sin(Li) * sinh(Li * x) *
Li ^ 2).*(sin(Lj * x) + 0.1e1 / sinh(Lj) * sin(Lj) * sinh(Lj * x)));
elseif strcmp(BC,'pinned+c') == 1
    y = sum(w.*(c * (sin(Li) + sinh(Li)) / (0.2e1 * Li * sinh(Li) + c * cos(Li) + c
* cosh(Li)) * cos(Li * x) * Li ^ 2 + c * (sin(Li) + sinh(Li)) / (0.2e1 * Li *
sinh(Li) + c * cos(Li) + c * cosh(Li)) * cosh(Li * x) * Li ^ 2 - sin(Li * x) * Li ^
2 - 0.1e1 / (0.2e1 * Li * sinh(Li) + c * cos(Li) + c * cosh(Li)) * (-0.2e1 *
sin(Li) * Li + c * cos(Li) + c * cosh(Li)) * sinh(Li * x) * Li ^ 2).*(-c * (sin(Lj)
+ sinh(Lj)) / (0.2e1 * Lj * sinh(Lj) + c * cos(Lj) + c * cosh(Lj)) * cos(Lj * x) +
c * (sin(Lj) + sinh(Lj)) / (0.2e1 * Lj * sinh(Lj) + c * cos(Lj) + c * cosh(Lj)) *
cosh(Lj * x) + sin(Lj * x) - 0.1e1 / (0.2e1 * Lj * sinh(Lj) + c * cos(Lj) + c *
cosh(Lj)) * (-0.2e1 * sin(Lj) * Lj + c * cos(Lj) + c * cosh(Lj)) * sinh(Lj * x)));
elseif strcmp(BC,'free+c+k') == 1
    y = sum(w.*((-Li ^ 4 * sin(Li) + c * k * sin(Li) + Li ^ 4 * sinh(Li) + c * k *
sinh(Li) + 0.2e1 * Li ^ 3 * cosh(Li) * c) / (-cos(Li) * Li ^ 4 + cos(Li) * c * k +
cosh(Li) * Li ^ 4 + cosh(Li) * c * k + 0.2e1 * Li * sinh(Li) * k) * cos(Li * x) *
Li ^ 2 - (0.2e1 * Li ^ 3 * cos(Li) * c - Li ^ 4 * sin(Li) - c * k * sin(Li) + Li ^
4 * sinh(Li) - c * k * sinh(Li)) / (-cos(Li) * Li ^ 4 + cos(Li) * c * k + cosh(Li)
* Li ^ 4 + cosh(Li) * c * k + 0.2e1 * Li * sinh(Li) * k) * cosh(Li * x) * Li ^ 2 -
sin(Li * x) * Li ^ 2 - 0.1e1 / (-cos(Li) * Li ^ 4 + cos(Li) * c * k + cosh(Li) * Li
^ 4 + cosh(Li) * c * k + 0.2e1 * Li * sinh(Li) * k) * (cos(Li) * Li ^ 4 + cos(Li) *
c * k - cosh(Li) * Li ^ 4 + cosh(Li) * c * k - 0.2e1 * Li * sin(Li) * k) * sinh(Li
* x) * Li ^ 2).*(-(-Lj ^ 4 * sin(Lj) + c * k * sin(Lj) + Lj ^ 4 * sinh(Lj) + c * k
* sinh(Lj) + 0.2e1 * Lj ^ 3 * cosh(Lj) * c) / (-cos(Lj) * Lj ^ 4 + cos(Lj) * c * k
+ cosh(Lj) * Lj ^ 4 + cosh(Lj) * c * k + 0.2e1 * Lj * sinh(Lj) * k) * cos(Lj * x) -
(0.2e1 * Lj ^ 3 * cos(Lj) * c - Lj ^ 4 * sin(Lj) - c * k * sin(Lj) + Lj ^ 4 *
sinh(Lj) - c * k * sinh(Lj)) / (-cos(Lj) * Lj ^ 4 + cos(Lj) * c * k + cosh(Lj) * Lj
^ 4 + cosh(Lj) * c * k + 0.2e1 * Lj * sinh(Lj) * k) * cosh(Lj * x) + sin(Lj * x) -
0.1e1 / (-cos(Lj) * Lj ^ 4 + cos(Lj) * c * k + cosh(Lj) * Lj ^ 4 + cosh(Lj) * c * k
+ 0.2e1 * Lj * sinh(Lj) * k) * (cos(Lj) * Lj ^ 4 + cos(Lj) * c * k - cosh(Lj) * Lj
^ 4 + cosh(Lj) * c * k - 0.2e1 * Lj * sin(Lj) * k) * sinh(Lj * x)));
```

Continued

```
elseif strcmp(BC,'free') == 1
    y = sum(w.*(cosh(Li * x) * Li ^ 2 - cos(Li * x) * Li ^ 2 - (cosh(Li) - cos(Li))
/ (sinh(Li) - sin(Li)) * (sinh(Li * x) * Li ^ 2 - sin(Li * x) * Li ^ 2)).*(cosh(Lj
* x) + cos(Lj * x) - (cosh(Lj) - cos(Lj)) / (sinh(Lj) - sin(Lj)) * (sinh(Lj * x) +
sin(Lj * x))));
elseif strcmp(BC,'pinned-pinned') == 1
    y = sum(w.*(-sqrt(0.2e1) * sin(Li * x) * Li ^ 2).*(sqrt(0.2e1) * sin(Lj * x)));
end
```

D.3.4 Function phi2_phi_x

```
function y = phi2_phi_x(BC,Li,Lj,c,k)

N = 199;
h = 1/(N-1);
x = (0:h:1);
w = ones(1,N);
w(2:2:N-1) = 4;
w(3:2:N-2) = 2;
w = w*h/3;

if strcmp(BC,'clamped') == 1
    y = sum(w.*(x-1).*(cosh(Li * x) * Li ^ 2 + cos(Li * x) * Li ^ 2 - (sinh(Li) -
sin(Li)) / (cosh(Li) + cos(Li)) * (sinh(Li * x) * Li ^ 2 + sin(Li * x) * Li ^
2)).*(cosh(Lj * x) - cos(Lj * x) - (sinh(Lj) - sin(Lj)) / (cosh(Lj) + cos(Lj)) *
(sinh(Lj * x) - sin(Lj * x))));
elseif strcmp(BC,'pinned') == 1
    y = sum(w.*(x-1).*(-sin(Li * x) * Li ^ 2 + 0.1e1 / sinh(Li) * sin(Li) * sinh(Li
* x) * Li ^ 2).*(sin(Lj * x) + 0.1e1 / sinh(Lj) * sin(Lj) * sinh(Lj * x)));
elseif strcmp(BC,'pinned+c') == 1
    y = sum(w.*(x-1).*(c * (sin(Li) + sinh(Li)) / (0.2e1 * Li * sinh(Li) + c *
cos(Li) + c * cosh(Li)) * cos(Li * x) * Li ^ 2 + c * (sin(Li) + sinh(Li)) / (0.2e1
* Li * sinh(Li) + c * cos(Li) + c * cosh(Li)) * cosh(Li * x) * Li ^ 2 - sin(Li * x)
* Li ^ 2 - 0.1e1 / (0.2e1 * Li * sinh(Li) + c * cos(Li) + c * cosh(Li)) * (-0.2e1 *
sin(Li) * Li + c * cos(Li) + c * cosh(Li)) * sinh(Li * x) * Li ^ 2).*(-c * (sin(Lj)
+ sinh(Lj)) / (0.2e1 * Lj * sinh(Lj) + c * cos(Lj) + c * cosh(Lj)) * cos(Lj * x) +
c * (sin(Lj) + sinh(Lj)) / (0.2e1 * Lj * sinh(Lj) + c * cos(Lj) + c * cosh(Lj)) *
cosh(Lj * x) + sin(Lj * x) - 0.1e1 / (0.2e1 * Lj * sinh(Lj) + c * cos(Lj) + c *
cosh(Lj)) * (-0.2e1 * sin(Lj) * Lj + c * cos(Lj) + c * cosh(Lj)) * sinh(Lj * x)));
```

Continued

```
elseif strcmp(BC,'free+c+k') == 1
    y = sum(w.*(x-1).*((-Li ^ 4 * sin(Li) + c * k * sin(Li) + Li ^ 4 * sinh(Li) + c
* k * sinh(Li) + 0.2e1 * Li ^ 3 * cosh(Li) * c) / (-cos(Li) * Li ^ 4 + cos(Li) * c
* k + cosh(Li) * Li ^ 4 + cosh(Li) * c * k + 0.2e1 * Li * sinh(Li) * k) * cos(Li *
x) * Li ^ 2 - (0.2e1 * Li ^ 3 * cos(Li) * c - Li ^ 4 * sin(Li) - c * k * sin(Li) +
Li ^ 4 * sinh(Li) - c * k * sinh(Li)) / (-cos(Li) * Li ^ 4 + cos(Li) * c * k +
cosh(Li) * Li ^ 4 + cosh(Li) * c * k + 0.2e1 * Li * sinh(Li) * k) * cosh(Li * x) *
Li ^ 2 - sin(Li * x) * Li ^ 2 - 0.1e1 / (-cos(Li) * Li ^ 4 + cos(Li) * c * k +
cosh(Li) * Li ^ 4 + cosh(Li) * c * k + 0.2e1 * Li * sinh(Li) * k) * (cos(Li) * Li ^
4 + cos(Li) * c * k - cosh(Li) * Li ^ 4 + cosh(Li) * c * k - 0.2e1 * Li * sin(Li) *
k) * sinh(Li * x) * Li ^ 2).*(-(-Lj ^ 4 * sin(Lj) + c * k * sin(Lj) + Lj ^ 4 *
sinh(Lj) + c * k * sinh(Lj) + 0.2e1 * Lj ^ 3 * cosh(Lj) * c) / (-cos(Lj) * Lj ^ 4 +
cos(Lj) * c * k + cosh(Lj) * Lj ^ 4 + cosh(Lj) * c * k + 0.2e1 * Lj * sinh(Lj) * k)
* cos(Lj * x) - (0.2e1 * Lj ^ 3 * cos(Lj) * c - Lj ^ 4 * sin(Lj) - c * k * sin(Lj)
+ Lj ^ 4 * sinh(Lj) - c * k * sinh(Lj)) / (-cos(Lj) * Lj ^ 4 + cos(Lj) * c * k +
cosh(Lj) * Lj ^ 4 + cosh(Lj) * c * k + 0.2e1 * Lj * sinh(Lj) * k) * cosh(Lj * x) +
sin(Lj * x) - 0.1e1 / (-cos(Lj) * Lj ^ 4 + cos(Lj) * c * k + cosh(Lj) * Lj ^ 4 +
cosh(Lj) * c * k + 0.2e1 * Lj * sinh(Lj) * k) * (cos(Lj) * Lj ^ 4 + cos(Lj) * c * k
- cosh(Lj) * Lj ^ 4 + cosh(Lj) * c * k - 0.2e1 * Lj * sin(Lj) * k) * sinh(Lj *
x)));
elseif strcmp(BC,'free') == 1
    y = sum(w.*(x-1).*(cosh(Li * x) * Li ^ 2 - cos(Li * x) * Li ^ 2 - (cosh(Li) -
cos(Li)) / (sinh(Li) - sin(Li)) * (sinh(Li * x) * Li ^ 2 - sin(Li * x) * Li ^
2)).*(cosh(Lj * x) + cos(Lj * x) - (cosh(Lj) - cos(Lj)) / (sinh(Lj) - sin(Lj)) *
(sinh(Lj * x) + sin(Lj * x))));
elseif strcmp(BC,'pinned-pinned') == 1
    y = sum(w.*(x-1).*(-sqrt(0.2e1) * sin(Li * x) * Li ^ 2).*(sqrt(0.2e1) * sin(Lj
* x)));
end
```

Appendix E

Complete Set-up of the Galerkin Method

The complete nondimensional equation of motion used throughout the thesis for a pipe conveying fluid was described by the following variables:

$$\eta = \frac{w}{L}\,, \quad \xi = \frac{x}{L}\,, \quad \tau = \left(\frac{EI}{m+M}\right)^{\frac{1}{2}} \frac{t}{L^2}\,. \tag{E.1}$$

All other parameters and constants involved are also made dimensionless and the general equation of motion of the system takes the following form

$$\alpha\dot{\eta}'''' + \eta'''' + \{u^2 + \gamma(\xi - 1)\}\eta'' + 2u\beta^{\frac{1}{2}}\dot{\eta}' + \gamma\eta' + \sigma\dot{\eta} + \ddot{\eta} = 0\,, \tag{E.2}$$

where

$$(\,)' = \frac{\partial}{\partial\xi}\,, \quad \dot{(\,)} = \frac{\partial}{\partial\tau}, \tag{E.3}$$

and

$$\begin{gathered} u = \left(\frac{M}{EI}\right)^{\frac{1}{2}} UL\,, \quad \beta = \frac{M}{m+M}, \quad \gamma = \frac{(M+m)L^3 g}{EI}\,, \\ \alpha = \left[\frac{I}{E(m+M)}\right]^{\frac{1}{2}} \frac{E^*}{L^2}\,, \quad \sigma = \frac{c^* L^2}{[EI(m+M)]^{\frac{1}{2}}}. \end{gathered} \tag{E.4}$$

The set-up of the Galerkin method for this problem has the following derivation:

$$\eta = \sum_{\mathrm{i}=1}^{\mathrm{N}} \phi_{\mathrm{i}}(\xi)\mathrm{P}_{\mathrm{i}}(\tau)\,, \frac{\partial^4\phi_i}{\partial\xi^4} = \lambda_i^4\phi_i\,, \text{ plug into EOM} \tag{E.5}$$

$$\sum_{i=1}^{N}\left[\lambda_i^4\phi_i P_i + \alpha\lambda_i^4\phi_i\dot{P}_i + u^2\phi_i{}'' P_i + 2\,u\,\beta^{\frac{1}{2}}\phi_i'\dot{P}_i + \gamma\phi_i' P_i + \gamma(\xi-1)\phi_i'' P_i + \sigma\phi_i\dot{P}_i\right.$$

$$\left. + \phi_i\ddot{P}_i\right] = 0 \rightarrow \text{Multiply by } \varphi_j \text{and integrate from 0 to 1}$$

$$\sum \lambda_i^4 P_i \int_0^1 \phi_i\phi_j\,d\xi + \sum \alpha\lambda_i^4\dot{P}_i \int_0^1 \phi_i\phi_j\,d\xi + \sum u^2 P_i \int_0^1 \phi_i''\phi_j\,d\xi + \sum 2\,u\,\beta^{\frac{1}{2}}\dot{P}_i \int_0^1 \phi_i'\phi_j\,d\xi$$

$$+ \sum \gamma P_i \int_0^1 \phi_i'\phi_j\,d\xi + \sum \gamma P_i \int_0^1 \phi_i''\phi_j(\xi-1)\,d\xi + \sum \sigma\dot{P}_i \int_0^1 \phi_i\phi_j\,d\xi$$

$$+ \sum \ddot{P}_i \int_0^1 \phi_i\phi_j\,d\xi = 0$$

$$\int_0^1 \phi_i\phi_j\,d\xi = \int_0^1 \phi_i{}''\phi_j{}''\,d\xi = \begin{cases} 0, i \neq j \\ \Psi, i = j \end{cases}$$

The derivation described by equation (E.5) is then used to set-up the matrices described in the Matlab ® program. Note that, in this particular case, Ψ is used to describe the integral of the product of two identical comparison functions. This is because the comparison functions used are not necessarily normalized, meaning that all integrals shown in equation (E.5) should be computed every time to avoid any conceptual error.

Bibliography

Gregory, R. W., & Paidoussis, M. P. (1966a). Unstable oscillation of tubular cantilevers conveying fluid. *Proceedings of the Royal Society (London)* (293), 512-527.

Guran, A., & Plaut, R. H. (1994). Stability of a Fluid-Conveying Pipe With Flow-Dependent Support Stiffness. *Journal of Applied Mechanics , 61*, 477-478.

Guran, A., & Plaut, R. (1993). Stability boundaries for fluid-conveying pipes with flexible support under axial load. *Archive of Applied Mechanics , 64*, 417-422.

Jamin, S. (2010). *Stability of Thick and Thin Flexible Pipes Subjected to Axial Flow.* McGill University, Department of Mechanical Engineering. Montreal: McGill University.

Karnovsky, I. A., & Lebed, O. I. (2004). *Free Vibrations of Beams and Frames: Eigenvalues and Eigenfunctions.* New York: McGraw-Hill.

Kiusalaas, J. (2005). *Numerical Methods In Engineering With Matlab.* New York: Cambridge University Press.

Paidoussis, M. P. (1998). *Fluid-Structure Interactions: Slender Structures and Axial Flow* (Vol. 1). Montreal, Quebec: Academic Press.

Paidoussis, M. P. (1998). *Fluid-Structure Interactions: Slender Structures and Axial Flow* (Vol. 2). Montreal, Quebec: Academic Press.

Paidoussis, M. P., & Des Trois Maisons, P. E. (1971). Free vibration of a heavy, damped, vertical cantilever. *Journal of Applied Mechanics , 38*, 524-526.

Rinaldi, S. (2009). *Experiments on the dynamics of cantilevered pipes subjected to internal and/or external axial flow*. McGill University, Department of Mechanical Engineering. Montreal: McGill University.